Modeling the Actin.myosin ATPase Cross-bridge Cycle for Skeletal and Cardiac Muscle Myosin Isoforms

Srboljub M. Mijailovich[1], Djordje Nedic[2], Marina Svicevic[2], Boban Stojanovic[2] Jonathan Walklate[3], Zoltan Ujfalusi[3], and Michael A. Geeves[3]

[1]Dept. of Chemistry and Chemical Biology Northeastern University, Boston, MA 02115, USA,

[2]Faculty of Science, University of Kragujevac, Kragujevac, Serbia,

[3]Dept. of Biosciences, University of Kent, Canterbury, Kent CT2 7NJ, UK,

[4]Dept. of Mechanical Engineering, Wenthworth Institute of Technology, MA 02115, USA

Jan. 23, 2017

Running Head: Modeling actin.myosin ATPase cycle

Address for correspondence:

Srboljub M. Mijailovich
Northeastern University
Department of Chemistry
207 Hurtig Hall
334 Huntington Ave
Boston, MA 02115, USA

Tel: (1) 617.373.2832
Fax: (1) 617.373.8795
smijailo@gmail.com

ABSTRACT

Modeling the complete actin.myosin ATPase cycle has always been limited by the lack of experimental data concerning key steps of the cycle because these steps can only be defined at very low ionic strength. Here using the human beta-cardiac myosin-S1 we combine published data from transient and steady-state kinetics to model a minimal eight state ATPase cycle. The model illustrates the occupancy of each intermediate around the cycle and how the occupancy is altered by changes in actin concentration for [actin] = 1-20 Km. The cycle can be used to predict the maximum velocity of contraction (motility assay or sarcomeric shortening) at different actin concentrations (which are consistent with experimental velocity data) and predict the effect of a 5 pN load on a single motor. The same exercise was repeated for the human alpha-cardiac myosin S1 and rabbit fast skeletal muscle S1. The data illustrates how the motor domain properties can alter the ATPase cycle and hence the occupancy of the key states in the cycle. These in turn alter the predicted mechanical response of the myosin independent of other factors present in a sarcomere such as filament stiffness and regulatory proteins. We also explore the potential of this modeling approach for the study of mutations in human beta cardiac myosin using the hypertrophic myopathy mutation R453C. Our modeling, using the transient kinetic data of Bloemink et al. (2014, J. Biological Chemistry 289:5158-516) predicts the mechanical properties of the motor that are compatible with the single molecule study of Sommese et al. (2013, PNAS 110:12607-12612). The modeling approach may therefore be of wide use for prediciting the properties of myosin mutations.

Keywords: myosin-S1 binding, load dependence, modeling

INTRODUCTION

The actomyosin ATPase cycle has been studied since myosin was first isolated and recognised as an ATPase (1-3). The biochemical kinetics of the cycle have been defined using steady-state and transient kinetics methods for different myosin isoforms (both muscle and non-muscle) and under a range of different experimental conditions (4, 5). The major events around the cycle remain the same for all myosins studied to date (see Fig. 1) but with alterations in the overall cycle speed and the fraction of the cycle time spent in the different intermediates around the cycle, e.g. the duty ratio (6-8). These alterations in the cycle tune the myosin to a specific function which for the sarcomeric myosin IIs include shortening velocity, steady-state force and efficiency defined as force per ATP etc. (9). While these results have led to a good understanding of the molecular and structural changes in the cycle understanding how these operate in the cell is often more difficult. Two missing elements in any model of the cycle in solution are how load on the motor alters the cycle and the effective actin concentration the myosin is exposed to. Any model of the cross bridge cycle has to build in these two elements to create a description of the working system. We present here a cross bridge model which examines these two elements in relation to the differences between the major muscle myosin II isoforms, fast skeletal myosin (rabbit myosin 2a) and the two human cardiac isoforms α and β. The β-cardiac isoform is identical to the slow muscle isoform.

We have recently completed a kinetic analysis of the slow skeletal/ β-cardiac muscle isoform of both bovine (10) and human myosin II (11). The step size and load dependence of the ADP release step has recently been defined for the human and porcine β-cardiac isoform (12, 13). It is therefore a good time to attempt to model the complete ATPase cycle for this well-defined slow muscle isoform (MyHC-7) and compare it with the closely related faster isoforms, i.e. the isoform found in the human atrium, α-cardiac, (MyHC6) which we have also studied (11) and the well characterised fast skeletal 2a isoform from rabbit (MyHC2).

The work presented here is part of a broader effort to develop a suite of programmes (MUSICO) that can model different aspects of muscle contraction from the molecular interaction of individual proteins through to the contracting muscle fiber. Here the ATPase cycle is modeled as a first step in this process. For a quantitative understanding of the ATPase in solution the data analysis should be performed on actomyosin-ATPase cycle model with a sufficient number of

states as, for example the minimum cycle set out in Fig. 1. In this ATPase cycle there are 8 intermediates defined by 9 equilibrium and 18 rate constants. Since the rate and equilibrium constants are not independent only 18 constants are required for a complete description of the cycle. From the published transient kinetic studies it is possible to define many of the constants. As set out in the methods for the β-myosin and listed in Table S1 three forward rate constants (k_{D^*}, k_{T^*}, k_H) and two equilibrium constants (K_T and $K_D K_{D^*}$) can be measured with precision of at least 20%. Three steps are defined as diffusion limited with a minimum value of 10^7 $M^{-1}s^{-1}$ (k_A, k_T and k_{-D}), and two other events are estimated to be too fast to measure and therefore have little influence on the modeling ($k_{T^{**}}$, k_{-A}), which together allows one equilibrium constant and three rate constants to be defined by detailed balance (K_T, k_D, k_{-D^*}, k_{-T}). The remaining 5 constants (K_A, K_H, K_{AH}, and the rate constants k_{-Pi} and k_{-T}) can be defined by fitting the model to the actin dependence of the steady state ATPase data and this analysis is presented here.

The experimental data used show clear differences in the three myosin isoforms. Our modeling illustrates how the properties of the isolated motor define the overall properties of the cycle, and how the myosin isoform can define the velocity at which the myosins can move actin, the load dependence of the cycle and the force generating capacity. In broad-brush terms the predictions based on simple solution kinetic measurements are compatible with the known properties of muscle fibers expressing these isoforms. Exact matching of the model to the data is not to be expected since additional parameters come in to play in the contracting muscle fiber such as the relative geometry of the actin myosin filaments, the stiffness of the structural elements and the ancillary proteins such as troponin, titin and myosin binding protein C. Thus, our aim here is not to match the fiber properties precisely but to explore the extent to which the myosin isoform properties themselves define the contraction properties of the sarcomere.

METHODS

The rate kinetic process for ATP cycle shown in Fig. 1 can be described as a system of linear equations that define the rate of change in state concentration as a function of the instantaneous fluxes between the states:

$$d\mathbf{C}/dt = \mathbf{K}\,\mathbf{C} \qquad (1)$$

Where **C** is a vector of the eight state concentrations form ATP-ase cycle (Fig. 1), i.e. $\mathbf{C} = \{[\text{MDPi}], [\text{A-MDPi}], [\text{AMD}], [\text{AM-D}], [\text{AM}], [\text{AMT}], [\text{A-MT}], [\text{MT}]\}^T$, and **K** is a matrix defining the state transition rates from and into each state. The general solution of this system of equation provides the transient response of each state from an initial state to the steady state solution. However, the matrix **K** is singular because the sum of all the rows is a row of zeroes, and therefore the determinant of $|\mathbf{K}| = 0$. Thus, for unique solution of Eq. 1, it is necessary to replace in **K** one row by the constraint equation coefficients derived from preservation of myosin species, i.e. the sum of concentrations of all states containing myosin should be equal to total myosin concentration $[\text{M}_{\text{tot}}]$ at any instant t (14-16):

$$\mathbf{K} = \begin{array}{c} \begin{matrix} \text{MDPi} & \text{A-MDPi} & \text{AMD} & \text{AM-D} & \text{AM} & \text{AMT} & \text{A-MT} & \text{MT} \end{matrix} \\ \begin{bmatrix} -k_A[A] - k_{-H} & k_{-A} & 0 & 0 & 0 & 0 & 0 & k_H \\ k_A[A] & -k_{-A} - k_{Pi} - k_{AH} & k_{-Pi}[Pi] & 0 & 0 & 0 & k_{-AH}[A] & 0 \\ 0 & k_{Pi} & -k_{-Pi}[Pi] - k_{D^*} & k_{-D^*} & 0 & 0 & 0 & 0 \\ 0 & 0 & k_{D^*} & -k_{-D^*} - k_D & k_{-D}[ADP] & 0 & 0 & 0 \\ 0 & 0 & 0 & k_D & -k_{-D}[DP] - k_T[TP] & k_{-T} & 0 & 0 \\ 0 & 0 & 0 & 0 & k_T[TP] & -k_{T^*} - k_{-T} & k_{-T^*} & 0 \\ 0 & k_{AH} & 0 & 0 & 0 & k_{T^*} & -k_{T^{**}} - k_{-T^*} - k_{-AH}[A] & k_{-T^{**}}[A] \\ 1 & 1 & 1 & 1 & 1 & 1 & 1 & 1 \end{bmatrix} \end{array}$$

In the steady state, the increment in state concentration is equal to zero, i.e. $d\mathbf{C}/dt = 0$, and after inclusion of the conservation of myosin species constraint the steady state concentrations can be calculated from:

$$\mathbf{C} = \mathbf{K}^{-1}\,\mathbf{B} \qquad (2)$$

where the vector $\mathbf{B} = (0, 0, 0,\ 0,\ 0, 0, 0,\ [\text{M}_{\text{tot}}])^T$ includes the total concentration of myosin that is typically input parameter. The system of equations (Eq.2) is nonlinear because the state transition rates k_A, $k_{-T^{**}}$ and k_{-AH} depend on the concentration of available

actin sites, [A], that is a priori unknown, but for a known number of myosins bound to actin (in 6 actin-myosin states), the concentration of available actin sites can be calculated from:

$$[\mathrm{A}] = [\mathrm{A_{tot}}] - ([\text{A-MDPi}] + [\text{AMD}] + [\text{AM-D}] + [\text{AM}] + [\text{AMT}] + [\text{A-MT}])$$

Thus, the concentration [A] can only be obtained iteratively. The first order differential Eq. 2 is solved numerically by a forward iterative procedure. Setting the initial value for [A] = [Atot], in each time step, after updating [A] in each iteration, the solution of Eq. 2 is typically obtained in less than twenty iterations.

Parameter estimation methods

There are many different methods for estimating parameters by fitting experimental data for example widely used global fitting KinTek Explorer (17-19). This global fitting software is successfully used for estimating rate and equilibrium constants a ATPase by globally fitting transient kinetic data of the Dbp5 ATPase cycle (20). However the global fitting methods may not be appropriate for fitting the experiments with simulations requiring a long time for each iteration and very large number of iterations thus we have developed several methods for the estimation of the model parameters for fitting kinetics data (21). The effective method for parameter estimation is the Damped Least Square (DLS) method, i.e. Levenberg–Marquardt inversion, because of two important features: a quantitative evaluation of the uniqueness of the estimated parameters and the degree of parameter interdependence via a parameter resolution matrix (21, 22). The DLS method is based on the iterative minimization of the mean-square error of the model predictions with respect to experimental observations. In this study, we estimate the rate transition constants of the ATPase cycle shown in Fig. 1, by minimizing the variance between the predicted steady state ATP-ase rates over a range of actin concentrations. The observations covered a range of independent variables, wide enough, to uniquely resolve the set of model parameters for each myosin isoform. These observations $\boldsymbol{d}_{\mathrm{obs}}([A])$ are represented by a set on N values of the ATP-ase rate sampled at discrete actin concentrations. The deviation of the model predictions from the experimental observations is represented by the mean-square-error that is an integral measure of the "goodness" of the model prediction fit to the observations. Minimization of the mean square function provides the set of (free) parameters that best fit the experimental data using the iterative procedure described in (21).

The sensitivity of the model responses to each of the estimated parameters is examined by the resolution matrix **R** (an $m \times m$ matrix) at convergence: when **R**~**I,** the estimated model

parameters are uniquely determined, whereas when the matrix **R** has appreciable non-zero off-diagonal elements, variations of a particular parameter can be compensated by adjustments of other parameters that fit the experimental data equally well suggesting that the parameters are interdependent and cannot be uniquely resolved. Furthermore, if all the elements in a row of the resolution matrix are small then the corresponding parameter cannot be estimated for the given data set because the error is affected very little, even by large changes in this parameter.

In DLS, the iterative process is stopped when the error and the norm of the increment of the estimated parameters are less than the prescribed respective tolerances. Also the maximal number of iterations is usually limited (here, the limit was 100) and the convergence is typically reached in 30-50 steps).

Estimation of rate constants

Choosing a set of rate constant for this study depends upon having a good estimate of the steady state ATPase data and a complete set of the rate constants for the cycle depicted in Fig 1. The problem is the conditions used for such measurement rarely match. The key ATP-ase measurements are obtained in solution by estimating the ATPase turnover rate, v as a function of varying actin concentration. These define V_{max} and K_m via the classical Michaelis-Menten equation, $v = V_{max}[A]/([A] + K_m)$. Actin activated ATPase assays require very low ionic strengths for the value of K_m to be in an accessible range of actin concentrations. ATPase assays cannot normally be performed at actin concentrations > 100 mM (5 mg/ml) because of the high viscosity of the solution and the excessive amounts of actin required. Thus ATPase assays are restricted to ionic strengths < 0.03M. In contrast, most assays of the cycle transient kinetics have used a much higher ionic strength to be close to those under physiological condition. Here we use complete fast kinetic data sets collected at 25 mM KCl and 100 mM KCl, for both the rabbit fast-skeletal muscle S1 (predominantly the 2a isoform) and human β-cardiac/slow skeletal isoform. ATPase data have been published for both proteins at 25 mM KCl (rabbit (23), beta β-cardiac (24)). The transient data for rabbit fast and human β-cardiac S1 at 100 mM KCl are from (11). The data for the beta cardiac S1 at 25 mM KCl was published in (25) and the rabbit data was collected specifically for this work using the identical approaches. The values used are listed in Table 1. The assignment of each rate and equilibrium constant is set out below for β-cardiac at 25 mM KCl and the same approach was taken to assign the values for other proteins (see Supporting Material for detailed information, Table S1).

For each step i in the cycle of Fig. 1 we can define $K_i = k_i/k_{-i}$ where K_i is the equilibrium constant of the ith step and k_i and k_{-i} are the forward and reverse rate constants (defined in a clockwise direction in Fig 1) respectively. Note the nomenclature for rate and equilibrium constants uses the subscript (A, D, Pi, T) to indicate the species binding or released from myosin in each 2nd order step. A star (*) indicates that it is an isomerisation event linked with the 2nd order binding or dissociation event. The only exception is K_H and K_{AH} which are the ATP hydrolysis steps with or without actin attached. Defining any two of the three parameters experimentally is sufficient; the third can be calculated from the first two. ATP binding occurs in two steps of which a rapid equilibrium step K_T which is defined experimentally in transient studies. The forward rate constant k_T is assumed to be diffusion limited (a nominal value of 10^7 $M^{-1}s^{-1}$ is assigned to all diffusion limited steps) and the reverse rate constant k_{-T} obtained by calculation k_{-T} = 10^7/ 3.06 x 10^3 = 3270 s^{-1} (illustrated for the β-cardiac myosin, see Table 1 for estimated value from the data fit). On ATP binding the actomyosin complex undergoes a rapid isomerization controlled by k_{T^*} which is measured as the limiting rate of ATP binding as 1540 s^{-1}. This is a largely irreversible step so the reverse rate constant, k_{-T^*}, is set at a nominal 10 s^{-1} giving K_{T^*} as 154. Actin then rapidly detaches with a rate constant, $k_{T^{**}}$, which is at least as fast as k_{T^*} and is set at a nominal 1000 s^{-1} and the reverse rate at 1 $\mu M^{-1}s^{-1}$, to give an affinity of actin for MT of ~ 1 mM about 10 fold weaker than that expected for MDPi. The rate constant for the ATP hydrolysis step is set either by quenched flow studies or as the maximum rate of the tryptophan fluorescence change on ATP binding to S1 having typical rate $k_H + k_{-H}$~15 s^{-1}. The equilibrium constant is not well defined but is thought to be between 1 and 10, and we have (initially) assigned k_H = 14 s^{-1} and k_{-H}= 1.4 s^{-1}, see Table 1 for estimated value from the data fit. Actin rebinding occurs from the M.ADP.Pi states and actin induces the release of Pi and the transition to the force developing strongly attached AMD sate. Neither of these steps can be easily distinguished from preceding or following steps in a direct assay. The values were therefore defined from the fit to the actin dependence of the steady state ATPase data.

A load dependent isomerization of AMD follows Pi release and the forward rate constant is directly measured for β S1 by displacing ADP by a large excess of ATP. This defines k_{D^*} as 59 s^{-1} and the amplitude analysis defines K_{D^*} as 0.167 and hence k_{-D^*} as 354 s^{-1}. This step is thought to define the maximum shortening velocity of muscle fiber contraction. It cannot be measured for rabbit muscle S1 as K_{D^*} is >> 1. Estimates of the value of this equilibrium

constant from Pi binding studies suggest a value of ~50 (26). The overall affinity of ADP for A.M, K_{dissn}, was measured by competition with ATP binding $K_{dissn} = K_D K_{D^*}/(1 + K_{D^*})$ to give the value of K_D listed. The ADP binding rate constant is assumed to be fast and diffusion limited while the ADP release is set at a nominal 1000 s^{-1}. All parameters used and calculated here are listed in Table 1 for each of the isoforms.

There is evidence that at high actin concentration, ATP hydrolysis and reversal of the recovery stroke can take place while myosin remains bound to actin, since if this were zero the ATPase rate would decline at very high actin concentrations (27). To allow for this we have included the step with equilibrium constant K_{AH}. We made no assumption about this step but allowed a value to be fitted within the limits of overall detailed balance of the two half cycles shown in Fig. 1.

Fitting data procedure

In order to quantitatively understand the ATP-ase process with the 8-state model shown in Fig. 1 it is necessary to know 18 rate or equilibrium constants. From multiple measurements and the analysis shown above it is possible to define 13 rate constants, thus the remaining 5 can be obtained by fitting the ATPase data by predictions of steady state ATPase from the solution of Eq. 2. Note when fitting to steady-state ATPase data in which initial rates are measured the concentration of ADP and Pi are assumed to be zero such that Pi and ADP release are irreversible. However, we include estimates of the two equilibrium constants K_{Pi} and K_{D^*} to allow a detailed balance calculation. Using known values of the rate constants in the cycle, we estimated unknown values of the equilibrium constants, K_A, K_H, K_{AH}, and the rate constants, k_{-Pi}, and, k_{-T}, by the DLS algorithm (21). The rapid convergence of parameters and the diagonal terms in the resolution matrix having values > 0.8 indicate well resolved and independent parameters.

RESULTS

Table 1 lists the rate and equilibrium constant for each of the steps in the cycle outlined in Fig. 1 for human β-cardiac motor domain (or S1). Where measured, each of these kinetic constants was defined at ~ 25 mM KCl and 20 °C, with a precision of at least 20%, others were assumed from known limits, i.e. diffusion limited, rapid equilibrium step or by detailed balance

as set out in the Methods section. The values undefined in the ATPase cycle are the affinity of actin for M.ADP.Pi complex (K_A in Fig 1) the rate and equilibrium constants of Pi release, K_{Pi}, and for human myosins the equilibrium constant of the ATP hydrolysis step. One other step not well defined is the affinity of the MT state for actin (K_{T**}) that is normally assumed to be very weak but since very high actin concentrations were modeled (as might be found in a sarcomere this affinity was set to 1 mM ~ 10 fold weaker than the actin affinity for MDPi (K_A)). We then also need to include values for the rate and equilibrium constants of the on-actin hydrolysis step (K_{AH}). We used published values for the steady state ATPase V_{max} and K_m for the same isoform (24) and fitted the model to the data (Fig. 2). The resulting fitted values are listed in bold in Table 1, and the convergence of fitted parameters for human β-cardiac-S1 is shown in Fig. 2B, and for rabbit fast skeletal, human cardiac α-S1 and human cardiac β-R453C-S1 in Fig. S1.

In Figure 2A the predicted ATPase rates as a function of actin concentration for human β-cardiac-S1 (based on the published V_{max} and K_m values) are shown as the blue circles and the red line is the best fit to the model. The convergence of the fitted parameters during the simulation is illustrated in Fig 2B and the resolution matrix for each fitted parameter is listed in Table 2. These show that the values rapidly converge and are all well-defined with exception of k_{-T}, the rate constant for ATP dissociation from the rigor A.M complex which is fast ~ 3000 s^{-1} and its precise value has little influence on the fitting process.

It is important to notice that the excellent fits do not guarantee that the parameters are uniquely defined. Having diagonal terms of order of 0.9 provides large confidence that the separation between parameters is very good, but not perfect (having value of 1). Off-diagonal terms <0.25 show only weak interdependence typical for fits of real data. However, the diagonal value of k_{-T} is very small implying that that from these data k_{-T} cannot be estimated and the small values from off-diagonal terms are irrelevant. This also suggests that using different values for k_{-T} may not affect the other estimated parameters because of small values of diagonal terms i.e. extremely weak interdependence.

Before considering the implication of the results we examined the robustness of the values used. For each of the fixed values (based on measurements or estimates; the non-bold values in Table 1) we changed the value by either +20% or -20% and refitted the ATPase data. In almost all cases case the fitted parameters changes by less than 2% only in the case of a change in K_D or K_{D^*} were larger changes seen, k_{Pi} and K_A changing by up to 7 % (see Table

S4). This indicates that the fitting is relatively independent of the fixed parameter values in the range ±20%. The same test was run for the fitted parameter values; i.e. we altered one of the fitted parameters (e.g. k_H) by ±20% and refitted the data. As can be seen from the fitted values in Table 1 both k_{Pi} and k_H have similar values, ~ 3× V_{max}, and contribute significantly to the overall ATPase V_{max}. Consequently an increase in k_H requires a decrease in k_{Pi} and visa-versa (See Table S5). A similar change in the actin affinity K_A was also required to fit the data. A change in K_H also requires a similar change in K_{AH} for thermodynamic balance. The quality of the fit judged by the error term (see Fig2B) remains very good. The errors reach the major minimum after ~ 10 iterations with small damped fluctuations in error afterwards concurrently displaying gradual convergence of the fitted values toward best fit solution. Thus, although the values are well defined by the fit, the values show some, typically minor, degree of dependence of each other.

Because these values may not be fully independent of each other we examined the influence of the 20% change in k_H and fitted values of k_{Pi} and K_A for the occupancy of the other states in the cycle. Since the overall ATPase rate (or the flux) does not change there is little change in any of the strongly attached states in the cycle (<1%). The effect is just a redistribution between [MT], [MDPi] and [A-MDPi] to maintain the same flux through this part of the cycle (see Table S6)

Figure 2A illustrates, in a pie-chart, the predicted occupancy of each of the states in the cross-bridge cycle model (each state color-coded to match Fig 1) for three actin concentrations [A] = K_m, $3K_m$ and $20K_m$ where the corresponding ATPase rates are 50%, 75% and 95% of V_{max} respectively. These three conditions were used to demonstrate how the cycle changes with increasing actin concentration. This also indicates how the situation my appear in an unloaded motility assay or rapidly contracting muscle fiber where the value and the meaning of actin concentration remains undefined because of the geometric constraints of the system. The pie-charts give a visual indication of how the occupancy of each of the cycle intermediates changes and allows an easy comparison between actin concentrations and different myosin isoforms (see below). Table S2 gives the calculated values for the state occupancy in each case, while Table 4 summarizes the changes in the sum of detached (red shades in Fig. 1), weakly (yellow shades) and strongly bound (blue shade) states. As expected, an increase in actin concentration results in a gradual shift from detached (MT and MDPi) to actin attached states with the detached MDPi

falling from 0.45 to 0.042 as the actin concentration increases from K_m to 20 K_m. The weakly attached A-MDPi state predominates (pale yellow, 0.36) at saturating actin concentrations and the sum of MT (dark red) and A-MT (dark yellow) giving a further 0.46. The only other highly occupied species is the strongly bound AMD complex (pale blue) which increase from 0.068 at [A] = K_m to 0.13 at [A] = 20 K_m.

Notably, the fraction of states that are strongly attached almost doubles from 0.073 to 0.141 as the actin concentration increases from K_m to 20 K_m. This fraction of strongly attached states is equal to the duty ratio, DR, i.e. the fraction of the ATPase cycle during which a cross bridge is strongly attached. This number then allows an estimate of the maximum velocity (in a motility assay or muscle shortening), V_o, from the equation $V_o = d/\tau$ where d is the myosin throw, i.e. the distance over which myosin can produce force, and τ is the lifetime of the attached state. The lifetime of the attached state is equal to DR/ATPase rate (the ATPase rates are also listed in Table 4 for each actin concentration), hence $V_o = d \times ATPase/DR$ The calculated values of V_o are listed in Table 4 and show that for a working stroke of 5 nm the velocity is ~0.20 μm.s^{-1}. The estimate of velocity is independent of the actin concentration above K_m, which is compatible with observations from the in vitro motility assays.

It is also possible to estimate the effect of a load on the ATPase cycle of a single myosin motor and this will be considered in the discussion. The model generates overall properties of the β-myosin isoform which are similar to those expected from contracting muscle fibers containing the isoform. In the next section the same approach is developed for a set of well-defined myosin isoforms.

Fast skeletal myosin S1 from the rabbit is the best biochemically defined fast muscle myosin and as illustrated in Fig 3A the fit of the model to the ATPase data was well defined. The resolution matrix indicated a similar quality of the fit (Table 3 and see Table S3 and Fig S1). The state occupancies are shown in Fig. 3B, Tables 4 and Table S2.

A further isoform that we have characterized is the human α-cardiac myosin (11), but this isoform has only been well defined at 100 mM KCl, i.e. at conditions where the actin dependence of the steady state ATPase cannot be measured with any precision. The effect of salt on each of the steps of the ATPase cycle is well defined for the rabbit fast muscle myosin and human β-cardiac data as listed in the Table S1. The differences between 25 and 100 mM KCl for the measured parameters are very similar for both proteins. The major effect of KCl

concentration, apart from the expected change in actin affinity, is on the equilibrium constants of ATP binding (K_T) which is ~3 fold weaker at 100 mM KCl for both rabbit skeletal and human cardiac S1. The effect on all other steps is modest in comparison. The exception is the ADP affinity which is quite distinct for the two myosins; ADP binding is weak (120 μM) and relatively independent of KCl for rabbit fast muscle S1 while it is much tighter and salt dependent for human β-myosin (~ 20 μM at 100 mM KCl; ~ 6 μM at 25 mM KCl). On the assumption that α-cardiac myosin is like rabbit fast muscle in its weak affinity for ADP the 100 mM KCl values of rate and equilibrium constants can be corrected to 25 mM KCl as shown in Table S1 and the 25 mM KCl data are listed in Table 1. The reliability of the assumptions made here will be considered in the Discussion. The actin dependence of the ATPase data has been defined for several α myosin isoforms and, in general, the V_{max} of the ATPase and the velocity of shortening is about 2-3 times that of the β-isoform from the same species under the same experimental conditions (28). Since separation of pure α and β isoforms is not simple we have assumed a 3 fold difference in the V_{max} of the ATPase. We therefore repeated the modeling for the α-cardiac data with values of constants listed in Table 1. Once again the ATPase data can be well defined with good definition of all fitted constants (Figs. 3A and S1; Tables 4, and S2).

The R453C mutation in β-cardiac myosin is a classic severe hypertrophic myopathy mutation which, without intervention, results in 50% mortality rate in heterozygotic carriers of the mutation by the of age 40 (29). We defined the properties of this mutation in the human β-cardiac myosin motor domain by transient kinetics (10), and steady-state kinetics, single molecule and ensemble mechanical data were collected by collaborators (25). The transient kinetic data were collected at 100 mM KCl and have been corrected to the 25 mM KCl – as was done for the α-cardiac data (see Table S1) and the fits to the ATPase data were once again very good (Figs. 3A and S1; Tables 4, and S2).

With the model well-defined by the experimental data for the three myosin isoforms we can consider the details of the model and how each isoform differs in the state occupancy of each intermediate in the ATPase cycle, the predicted velocities, duty ratios and how these depend upon actin concentration. There are many different comparisons to be drawn between the different data sets, only the major issues will be highlighted here and further consideration given to the isoform differences in the Discussion. Note that for these ATPase cycles the concept of a simple rate-limiting step does not apply, as has been recognized in enzymology for a number of

years. Multiple states contribute to the overall balance of the cycle and small changes in any step can and will alter the balance of events in the cycle. This is why understanding the role of individual point mutations in a myosin requires a detailed study of the cycle.

As seen for the β-cardiac myosin in all cases the state occupancies shift from detached (MT and MDPi) to attached states as the actin concentration increased. Even though the actin concentrations used in the simulation result in the same degree of saturation of the ATPase velocity each myosin isoform has a distinct distribution of states. At [A] = K_m ($v = 0.5V_{max}$) the rabbit skeletal myosin has fractional occupation of the detached states as 0.58, weakly attached at 0.35 and strongly attached as 0.075 (note the values are rounded to 2 significant digits here, resulting in the total being less than 1). Distributions within these categories are given in Table 4 and listed in more detail in Fig 3B and Table S2. β-cardiac myosin has identical state occupancy of the strongly attached state and hence the same duty ratio as the skeletal isoform, 0.073, but there is a lower occupancy of the weakly attached states, 0.20. This alteration is the balance of the cycle is caused by a reduction in the rate constants controlling both ADP release and ATP hydrolysis. The two together result in a slower cycling speed and a retained duty ratio. But the slower hydrolysis step results in a greater occupancy of the MT complex and lower A-MDPi. In contrast, the α isoform has a higher duty ratio than either β or skeletal 2A, 0.10, and a distribution between detached and weakly attached states similar to that of the skeletal isoform. As actin concentration increases the strongly attached states but the duty ratio remains the same for the skeletal and β isoforms, saturating at about 0.14 while the α isoform is higher at 0.19. Note the β-cardiac at 20Km actin has more than twice the fraction of detached states as the skeletal isoform due to the slower rate constant of the hydrolysis step and while α isoform is more similar to the skeletal isoform.

As for the β isoform, the ATPase rates and the duty ratio can be used to estimate the unloaded shortening velocity. From the data in Table 4, in each case the predicted velocity is independent of the actin concentration and the α isoform has a predicted velocity of 0.45 μm/s for a 5 nm step more than twice that of the β isoform, 0.20 μm/s. The skeletal isoform has a velocity twice that of the α isoform, 0.99 μm/s. The relative values here are similar to those measured for the same myosin isoforms in motility assays however it is difficult to find measurements for all three isoforms under identical conditions. Absolute values do vary from laboratory to laboratory. Most recent values are collected at higher temperatures of ~30-35 °C

and velocity has a very marked temperature dependence (30, 31). Values from the rat muscle isoforms give 0.62 μm/s for the slow β isoform and 2.6 μm/s for the fast 2a isoform at 20 °C and ~5 times faster at 30 °C (31). The rat isoforms are expected to be two fold faster than the human isoforms with rabbit isoforms in between those of rat and human (32).

The R453C mutation in human β-cardiac myosin results in severe HCM. Our published analysis of this mutation (10) indicated that the major changes were a reduction in the rate constants of the ATP hydrolysis step (k_H) and the isomerization controlling ADP release (k_{D^*}). Putting these numbers into the model along with the ATPase data of Sommese et al. (25) gave the following predictions. Compared to the wt β data the duty ratio was increased by ~ 59 % at each actin concentration while the predicted velocity of shortening was reduced by almost 50%. The increased duty ratio and slower velocity are both the result of the longer lifetime of the AMD state. The longer lived AMD state results in a higher occupancy of the force holding (AMD) state and therefore predicts a higher force capacity for this mutation than for the wt. This is compatible with measured single molecule force (increased by 50%), increased ensemble force and the reduced motility assay velocity (reduced by 36%) reported for this mutation by Sommese et al. (25).

DISCUSSION

Defining a precise ATPase cycle for muscle myosins is a first step towards developing an accurate multiscale model that can be used for interpreting single molecule mechanical measurements, motility assays, data from Ca^{2+} regulated ATPase models and contracting sarcomeres. The advantage of having a well-defined ATPase cycle is that the subsequent models are more highly constrained allowing focus on the key additional processes, including the geometry of the available myosin binding sites on actin (see Mijailovich et al. (33)), the effect of load on individual motors or on an ensemble and the modulation of the cycle events by regulatory systems. Such a model is under construction (MUSICO (33-41)) but such a model needs good experimental data for each different muscle systems collected as nearly as possible under identical experimental conditions (ionic strength, temperature and etc.). This is a challenge as ATPase assays, motility assays and muscle fiber mechanics all have their own preferred conditions. Transient kinetics can be collected under most solution conditions

provided the proteins are stable over the time course of the measurement and at temperatures from zero to 40 °C (42).

The experimental data used here for both human β-cardiac and rabbit fast muscle myosin were collected under very similar conditions and, as seen, the predictions for duty ratio for these two isoforms give a very similar answer. The R453C transient kinetic data were collected at a higher ionic strength than the ATPase data and then corrected to the lower ionic strength. The similar effects of salt on the parameters for wt β-cardiac and rabbit fast muscle suggest the corrections applied will be reasonably accurate. This is particularly so as the R453 residue is not a surface exposed residue and therefore unlikely to be influenced directly by the solution ionic strength. But confirming the R453C data at the lower ionic strength would be essential if the modeling of this mutant were to be taken further forward. Here the intention is to present the potential of this modeling approach.

The data for α-cardiac isoform has both the ionic strength corrections for the transient kinetic data and the ATPase data and were extrapolated from closely related studies. This data is therefore of lower reliability. Our primary reason for including it here is to emphasize the potential of the approach. There are very few studies of the atrial myosin from any source and the Deacon et al. (11) work is the only transient kinetic study of the atrial isoform from human or any other source. There are myofibril studies from atrial and ventricle tissue that predominantly express α or β myosin isoforms respectively and several studies of atrial and ventricular myosin ATPases and motilities have been reported (43-45). In any future detailed study of the atrial isoforms it would be helpful to match the experimental conditions to those used here to facilitate comparisons using this modeling approach.

We use as far as possible strict criteria for including experimental data in our analysis i.e. that a single pure myosin isoforms were used in all experiments and the data were collected under the same experimental conditions of temperature and ionic strength. Other comparative data exists which do not match the exact details. Of significance is the work of White and a series of colleagues making a direct measure of the rate constant for Pi release at saturating actin concentrations using the phosphate binding protein (46, 47). Under slightly different ionic strength condition they estimate Pi release to be 75-77 s^{-1} for rabbit S1 which is about twice our estimate of 45 s^{-1}. Similar measurements on porcine β-cardiac S1, a close analogue of human β-S1, estimates the Pi release to be 17 s^{-1} (48) which compares well with our estimate of 16 s^{-1}.

Note however our fitting approach does show a co-dependence of k_{Pi} on the rate of the ATP hydrolysis step k_H. In our current assays the measurement of Pi release requires larger quantities of protein than are currently accessible for the human proteins. In general our analysis is in broad agreement with the studies of White and colleagues and indicates that both k_{Pi} and k_H have a major influence on the V_{max} of the ATPase, the relative importance of each may vary with ionic strength and temperature.

Comparisons of isoforms

To a first approximation muscle fibers expressing a single myosin isoform differ markedly in the maximum velocity of contraction and much less so in the isometric force (when correction is made for the density of myofilaments in the muscle fibers (9, 49)). Alongside this, single molecule studies of myosin II isoforms suggest little variation in the step size, duty ratio or force per crossbridge between muscle myosin II isoforms (44) suggesting little change in crossbridge stiffness between myosin isoforms. Changes in contraction parameters between isoforms are therefore thought to be largely due to the velocity of the ATP drive cycle (the steady state ATPase cycle for an unloaded system), and how much load affects the cycle. The data presented here illustrates how the unloaded systems changes for the three isoforms considered in terms of cycle speed and duty ratio and from which we can predict the unloaded velocity (from a motility assay or muscle fiber contraction). We have also explored how a load might affect each cycle differently for a single myosin motor assuming no change in the crossbridge stiffness between isoforms. The load dependence of an ensemble of myosin motors could be subject to a variety of additional sources of compliance such as filament compliance.

The data indicate, as expected, that all three myosin isoforms are low duty ratio motors. Rabbit skeletal and human β-cardiac are almost identical in this respect with a duty ratio of 0.11 at an actin concentration equivalent to $3K_m$. The α isoform is slightly higher at 0.15 but the difference is moderate and could be due to differences in the experimental conditions used and the corrections applied. From the duty ratios and ATPase rates and a 5 nm step size the velocities were predicted and are compatible with those expected from experimental studies; 1-2 μm/s for the fast muscle (for a 5-10 nm crossbridge throw) and reduced by 50% for the α-isoform and 80% for the β-isoform (5, 44).

There have been two reports of the effect of load on the ADP release step from the β-isoform and both studies (12, 13) fitted their data to a model where the load dependence of the rate constant for ADP release $k(F)$ is defined by

$$k(F) = k_o\, e^{(-F\cdot\delta_{det}/k_B*T)}$$

where k_o is the rate constant for ADP release in the absence of load, F is the force on the crossbridge and δ_{det} is the distance to the transition state, k_B is Boltzmann's constant, and T is the temperature.

We took the simplest approach to examine how the cycle would be influenced by such a load on a single molecule (i.e. no cooperative effects that would apply in an ensemble system). We assumed, based on the single molecule measurements which give δ_{det} as approximately 0.9 nm, that a 5 pN load would reduce ADP release by a factor of 3. For simplicity we applied the same 3 fold reduction in the rate constant for the force generating transition coupled to Pi release (k_{Pi}). We assumed the same value of δ_{det} for all three isoforms in order to evaluate how the cycle itself influences the load dependence of the isoforms. Any change in δ_{det} or of the stiffness of the crossbridge would be additive effects upon those illustrated here.

The result for [A] = $3K_m$ (see Table 5) shows the load would have a very similar effect on the velocity for both cardiac isoforms falling by ~ 65% while for the fast muscle isoform the reduction is lower at 57%. This is as expected from well-defined force velocity curves from individual muscle fibers where the contraction velocity of slow β myosin muscle fibers has a greater sensitivity to load. Interestingly, our data predicts that the α isoform has a very similar sensitivity of velocity to load but maintains an approximately 2 fold higher ATPase cycling rate than the β-isoform. The effects on the ATPase cycling rates were different, α-cardiac and the fast muscle isoform are inhibited to the same extent (-61.4 %) while the β isoform is only slightly less inhibited by 56%. This difference in the effect of load in the ATPase and velocity emphasizes the decoupling of ATPase and velocity cycles as first pointed out by White and collaborators (50).

If the tightly bound ADP state AMD is considered as the primary force holding state then the effect of load on the occupancy of this state is of interest. For the fast muscle and the α-cardiac myosin isoforms the load increases the fractional occupancy of this state by ~ 15 % in both cases (from 0.074 and 0.135 in unloaded conditions respectively, see Tables 5 and S2)

while the β-isoform occupancy increases by 32.5 % (from 0.10) – emphasizing again the greater sensitivity of the β isoform to load.

One of the clear results from the modeling is that the predicted velocity is independent of actin concentration. This is a result of both the ATPase and the duty ratio having the same dependency on actin concentration thus $V_o = d \times ATPase/DR$ is independent of actin concentration. The actin dependence of the duty ratio results from the actin dependence of the cycling time (= 1/ATPase) while strongly attached lifetime τ is primarily controlled by ADP release rate constant and is independent of actin concentration. Thus the velocity only depends upon the strongly attached lifetime and is independent of the actin dependent ATPase rate.

In our modeling we used three different actin concentrations to explore how the balance of the cycle changes for different levels of actin activation. This raises the question of the appropriate actin concentration for comparison with a myosin in the sarcomere. Most models use an estimate for the fraction of myosin heads attached to actin (strongly bound or the sum of weak and strongly bound) in the contraction sarcomere. These vary from 1-5% strongly attached crossbridges in a rapidly shortening muscle to ~20% under isometric conditions. At the lowest concentrations modeled ([A] = K_m) the estimate of strongly attached bridges is 7-10% without load for all three wt isoforms, and the weakly attached bridges vary from 20-35% for different isoforms. Thus the average actin concentration "seen" by a myosin head in the sarcomere would be of the order of the K_m value for actin while rapidly shortening. Of course, individual myosin heads would be exposed to a wide range of apparent actin concentrations in an isometric fiber which is why we used the higher actin concentration of 3 K_m to model the effect of load. The load-bearing strongly attached heads are those that are most likely to bind actin at the specific filament overlap considered. These issues will be considered further in the sarcomeric version of this model (MUSICO (33)).

R453C

We include the data for one β-cardiac myosin mutation here to illustrate the potential power of the approach for dissecting the effect of point mutations on myosin activity. R453C is a severe hypertrophic cardiomyopathy mutation and our published analysis (10) of this mutation indicated a significant reduction in the rate of ATP hydrolysis step (k_H) and ADP release (k_{D^*}). Including these values into the model gave the following predictions. The velocity was reduced by 47%

compare to wt while the duty ratio increased by 60% and the occupancy of the AMD state increased from 0.102 to 0.169, a 66% increase (Table 4 and S2). Thus a muscle expressing only this isoform would be expected to contract more slowly and develop higher forces due the greater fraction of strongly attached force holding states. The influence of load, with the same assumptions as for the wt protein show 65.7% reduction in velocity similar to the 65% reduction for the wt and a slightly smaller reduction in the ATPase rate of 55.7% (61 % for wt) while the occupancy of the AMD state increased markedly by 32.8 % from 0.117 fraction occupancy compared to 32.5% for wt as shown in Table 5. These numbers can be compared to the motility and single molecule data for this mutant from Sommese et al. (25). They found that the single molecule force generation increased by 50% from 1.4 pN for the wt to 2.1 pN. This compares with our predicted 66% increase in the strongly attached AMD state or the 60% increase in duty ratio. In the motility assay Sommese et al. (25) reported that the velocity was reduced by 24% from 0.8 µm/s from the wt to 0.61 µm/s and the velocity was more readily inhibited by a load using an actin cross-linker. Our data suggest a larger 47% reduction in velocity compared to wt and while velocity is reduced by a similar percentage (65%) by a load of 5 pN for wt and R453C.

The data used here is all referenced to 25 mM KCl – lower than that found in a muscle fiber. The transient kinetic data in table S1 indicates how some of these steps are affected by salt but estimating salt effects on the actin affinity and Pi release steps remain inaccessible to solution measurements at physiological ionic strengths. Even some motility assays and single molecule assays are best performed at low salt because of the low probability of a cross bridge being bound to actin at the higher ionic strengths. Muscle fiber or myofibril studies provide information concerning these events but the assays report on ensemble behavior and are affected by the 3D geometry of the filaments. These require a different modeling approach (33), which is under development, but having the majority of the ATPase cycle well defined puts limits on the remaining variables in such models.

What we have demonstrated here is that studies of the unloaded solution ATPase cycle can define the properties of myosin isoforms and of mutations in the motor domain. Studies allow predictions and set limits on the mechanical behavior of each isoform. Each of the isoforms studied here has a specific relationship between the cycle and the predicted mechanical events which can define some of the properties of the contracting muscle fiber such as maximum velocity and load sensitivity. In the next stage of developing our multilevel modeling package (MUSICO) we will examine how the properties of the individual myosin isoforms defined here

modulate the calcium regulation of the thin filament and the mechanical properties of a contracting sarcomere. For example, the differences in the number and lifetimes of the strongly attached AMD cross-bridge for each isoform might be expected to influence the switching between on and off states of the thin filament.

SUPPORTING MATERIAL

One figure and six tables are available at http://www.biopysj/supplemental/XXXXXXX.

Author Contributions:

S.M.M. designed research, performed research, contributed to development of analytic tools, analyzed data and wrote the paper.

D.N. developed the computational tools.

M.S. contributed to the development of the computational tools, performed data fitting and data analysis.

B.S. supervised and coordinated development of computational tools, fitting data and data analysis.

J.W. contributed in data preparation and data analysis.

Z.U. contributed in data preparation and data analysis.

M.A.G. contributed to research design, data analysis and writing the paper.

ACKNOWLEDGEMENTS

This project was supported by NIH R01 grants AR048776 to S.M.M. and GM29090 to M.A.G. (subcontract of grant awarded to Leslie Lienwand) and a British Heart Foundation grant No PG30200 to M.A.G.. We also would like to thank for graceful (partial) support of Mijailovich family, especially Dragica Mijailovic, Esq. (LLM).

Figures Legends

FIGURE 1 A minimal ATPase actin-myosin cycle is defined by eight states and nine equilibrium constants. The actin monomers, A, along an actin filament are shown as three green filled circles and the motor domain of myosin, M, is represent as two ellipses, the large representing the upper and lower 50 k domain with a cleft separating the two. The smaller ellipse represents the converter domain with a rectangular lever arm. The relative movements of these domains represent the structural conformations of myosin in each state. The actin-myosin cycle includes ATP binding to rigor-like complex, AM, forming the AMT state (equilibrium constant for the transition K_T = [AMT]/[AM][T]) followed by a rapid change in myosin conformation leading to the cleft opening in the A-MT state (K_{T*}) and followed by rapid detachment of actin (K_{T**}). A conformation change in the head following the opening of the 50 kDa cleft leads to the recovery stroke and hydrolysis of ATP transitioning into the MDPi state (K_H). Then, the myosin can reattach to actin forming A-MDPi state (K_A) and after the cleft closure, the power stroke and Pi release transitioning into an AMD state (K_{Pi}) in which ADP remains firmly attached to myosin. This state allows a conformational change into the AM-D state (K_{D*}) from which ADP is released (K_D) and the cycle is completed. The step labelled K_{AH} allows for possible hydrolysis ATP while myosin remains attached to actin. For simplicity, ATP and ADP in state labeling are denoted as T and D, respectively, inorganic phosphate as Pi, and a hyphen indicates relatively weak association between the species. The equilibrium constants between the states are denoted in green letters and represent a ratio between forward (clockwise) and reverse state transition rate constants. Note the nomenclature for rate and equilibrium constants uses the subscript (A, D, Pi, T) to indicate the species binding or released from myosin in each 2nd order step. A star (*) indicates that it is an isomerisation event linked with the 2nd order binding or dissociation event. The only exception is K_H and K_{AH} which are the ATP hydrolysis steps with or without actin attached.

FIGURE 2 Modeling the ATPase cycle for β-cardiac myosin. (A) The best fit of ATP-ase vs. actin concentration [A] of HC WT β - S1. Data in black are the predicted ATPase rates based on the published V_{max} and K_m values and the red data are the best fit of the model in Fig. 1 to the data. The constants used and derived in the fitting are listed in Table 1. The state occupancies

for each of the intermediates in the cycle are given in a pie chart, color coded to match the intermediates in Fig 1. These are shown for 3 actin concentration (blue diamonds) at [A] = K_m, $3K_m$, $20K_m$ and at $3K_m$ under load – see text. B) The convergence of the equilibrium constants, K_A, K_H, , K_{AH}, and reverse rate constants, k_{-Pi}, and , k_{-T}, by DLS for the damping parameter ε=0.25 (21). All free parameters converge at 30 to 50 iterations except k_{-T} where value varies between 3200 and 3350 s^{-1} but, however, this variation does not affect the error suggesting that the value of this parameter cannot be resolved for this experiment (see Table 1). The mean square error (21) converges quickly to a normalized value, Error =$\sqrt{\|\mathbf{e}\|_2^2/N}$ <2×10^{-6} s^{-1}, and fit of data is excellent. The resolution matrix for this fitting procedure is listed in Table 2.

FIGURE 3 The details of the fit to the ATPase data (A) and the state occupancy of intermediates in the ATPase cycle (B) for four muscle myosin isoforms. A) The dependence of the ATPase cycle on actin concentration and B) the occupancy of each of the intermediates in the ATPase cycle at three different actin concentrations [A] =K_m, $3K_m$ and 20 K_m corresponding to 0.5, 0.75 and 0.95 of V_{max}. The presentation also includes predictions for how the state occupancy would change for the [A] = $3K_m$ conditions if the actomyosin system were loaded such that the isomerization steps controlling both Pi and ADP release were reduced by a factor of 3 (see text for details). The values generated for the pie charts are given in Table S2.

Note: Low actin concentration state occupancies were dominated by MDPi (range 0.40 to 0.45) and to a lesser extent by A-MDPi (0.19-0.32). The MT form was more variable (0.13-0.29) reflecting the wide variation in the rate constant of the ATP hydrolysis step (k_H). As actin increased, there was a shift in occupancy from MDPi to A-MDPi as expected with MDPi almost negligible at [A] =$20K_m$. A-MDPi dominates (0.35-0.62) at [A] = $20K_m$ but with significant contributions from both MT (0.06-0.26) and A-MT (0.14-0.21). The presence of a large amount of A-MT is due to the value of the weak affinity of MT for actin here assigned to 1 mM at 25 mM KCl and expected to be 3 times weaker at 100 mM KCl. Thus the A-MT would only be significant in a sarcomere if the local actin concentration exceeded 1mM at physiological salt concentrations. The occupancy of MT is much larger in beta than in alpha and skeletal isforms reflecting the slower hydrolysis rate constant for beta. The major form tightly bound to actin was AMD and this had a higher occupancy in beta and alpha than in skeletal myosin at all actin concentrations reflecting the slower ADP release rate constants (k_D) in the β and α-isoforms.

REFERENCES

1. Lymn, R. W., and E. W. Taylor. 1971. Mechanism of adenosine triphosphate hydrolysis by actomyosin. Biochemistry 10:4617-4624.
2. Trentham, D. R., J. F. Eccleston, and C. R. Bagshaw. 1976. Kinetic analysis of ATPase mechanisms. Quarterly reviews of biophysics 9:217-281.
3. Geeves, M. A. 1991. The dynamics of actin and myosin association and the crossbridge model of muscle contraction. The Biochemical journal 274 (Pt 1):1-14.
4. Bloemink, M. J., J. C. Deacon, D. I. Resnicow, L. A. Leinwand, and M. A. Geeves. 2013. The superfast human extraocular myosin is kinetically distinct from the fast skeletal IIa, IIb, and IId isoforms. The Journal of biological chemistry 288:27469-27479.
5. Resnicow, D. I., J. C. Deacon, H. M. Warrick, J. A. Spudich, and L. A. Leinwand. 2010. Functional diversity among a family of human skeletal muscle myosin motors. Proceedings of the National Academy of Sciences of the United States of America 107:1053-1058.
6. Bloemink, M. J., and M. A. Geeves. 2011. Shaking the myosin family tree: biochemical kinetics defines four types of myosin motor. Seminars in cell & developmental biology 22:961-967.
7. De La Cruz, E. M., and E. M. Ostap. 2004. Relating biochemistry and function in the myosin superfamily. Current opinion in cell biology 16:61-67.
8. Heissler, S. M., and J. R. Sellers. 2016. Kinetic Adaptations of Myosins for Their Diverse Cellular Functions. Traffic 17:839-859.
9. Bottinelli, R., and C. Reggiani. 2000. Human skeletal muscle fibres: molecular and functional diversity. Progress in biophysics and molecular biology 73:195-262.
10. Bloemink, M., J. Deacon, S. Langer, C. Vera, A. Combs, L. Leinwand, and M. A. Geeves. 2014. The hypertrophic cardiomyopathy myosin mutation R453C alters ATP binding and hydrolysis of human cardiac beta-myosin. The Journal of biological chemistry 289:5158-5167.
11. Deacon, J. C., M. J. Bloemink, H. Rezavandi, M. A. Geeves, and L. A. Leinwand. 2012. Erratum to: Identification of functional differences between recombinant human alpha and beta cardiac myosin motors. Cellular and molecular life sciences : CMLS 69:4239-4255.

12. Greenberg, M. J., H. Shuman, and E. M. Ostap. 2014. Inherent force-dependent properties of beta-cardiac myosin contribute to the force-velocity relationship of cardiac muscle. Biophysical journal 107:L41-44.
13. Sung, J., S. Nag, K. I. Mortensen, C. L. Vestergaard, S. Sutton, K. Ruppel, H. Flyvbjerg, and J. A. Spudich. 2015. Harmonic force spectroscopy measures load-dependent kinetics of individual human beta-cardiac myosin molecules. Nature communications 6:7931.
14. Smith, D. A., and M. A. Geeves. 1995. Strain-dependent cross-bridge cycle for muscle. Biophysical journal 69:524-537.
15. Smith, D. A., and M. A. Geeves. 1995. Strain-dependent cross-bridge cycle for muscle. II. Steady-state behavior. Biophysical journal 69:538-552.
16. Mijailovich, S. M., J. P. Butler, and J. J. Fredberg. 2000. Perturbed equilibria of myosin binding in airway smooth muscle: bond-length distributions, mechanics, and ATP metabolism. Biophysical journal 79:2667-2681.
17. Johnson, K. A., Z. B. Simpson, and T. Blom. 2009. FitSpace explorer: an algorithm to evaluate multidimensional parameter space in fitting kinetic data. Analytical biochemistry 387:30-41.
18. Johnson, K. A., Z. B. Simpson, and T. Blom. 2009. Global kinetic explorer: a new computer program for dynamic simulation and fitting of kinetic data. Analytical biochemistry 387:20-29.
19. Otto, M. R., M. P. Lillo, and J. M. Beechem. 1994. Resolution of multiphasic reactions by the combination of fluorescence total-intensity and anisotropy stopped-flow kinetic experiments. Biophysical journal 67:2511-2521.
20. Wong, E. V., W. Cao, J. Voros, M. Merchant, Y. Modis, D. D. Hackney, B. Montpetit, and E. M. De La Cruz. 2016. P(I) Release Limits the Intrinsic and RNA-Stimulated ATPase Cycles of DEAD-Box Protein 5 (Dbp5). Journal of molecular biology 428:492-508.
21. Mijailovich, S. M., X. Li, J. C. Del Alamo, R. H. Griffiths, V. Kecman, and M. A. Geeves. 2010. Resolution and uniqueness of estimated parameters of a model of thin filament regulation in solution. Comput. Biol. Chem. 34:19-33.
22. Menke, W. 1989. Geophysical Data Analysis: Discrete Inverse Theory. Academic Press, Inc., San Diego, CA.

23. Swenson, A. M., D. V. Trivedi, A. A. Rauscher, Y. Wang, Y. Takagi, B. M. Palmer, A. Malnasi-Csizmadia, E. P. Debold, and C. M. Yengo. 2014. Magnesium modulates actin binding and ADP release in myosin motors. The Journal of biological chemistry 289:23977-23991.
24. Nag, S., R. F. Sommese, Z. Ujfalusi, A. Combs, S. Langer, S. Sutton, L. A. Leinwand, M. A. Geeves, K. M. Ruppel, and J. A. Spudich. 2015. Contractility parameters of human beta-cardiac myosin with the hypertrophic cardiomyopathy mutation R403Q show loss of motor function. Science advances 1:e1500511.
25. Sommese, R. F., J. Sung, S. Nag, S. Sutton, J. C. Deacon, E. Choe, L. A. Leinwand, K. Ruppel, and J. A. Spudich. 2013. Molecular consequences of the R453C hypertrophic cardiomyopathy mutation on human beta-cardiac myosin motor function. Proceedings of the National Academy of Sciences of the United States of America 110:12607-12612.
26. Sleep, J. A., and R. L. Hutton. 1980. Exchange between inorganic phosphate and adenosine 5'-triphosphate in the medium by actomyosin subfragment 1. Biochemistry 19:1276-1283.
27. Stein, L. A., P. B. Chock, and E. Eisenberg. 1981. Mechanism of the actomyosin ATPase: effect of actin on the ATP hydrolysis step. Proceedings of the National Academy of Sciences of the United States of America 78:1346-1350.
28. Malmqvist, U. P., A. Aronshtam, and S. Lowey. 2004. Cardiac myosin isoforms from different species have unique enzymatic and mechanical properties. Biochemistry 43:15058-15065.
29. Watkins, H., A. Rosenzweig, D. S. Hwang, T. Levi, W. McKenna, C. E. Seidman, and J. G. Seidman. 1992. Characteristics and prognostic implications of myosin missense mutations in familial hypertrophic cardiomyopathy. The New England journal of medicine 326:1108-1114.
30. Anson, M. 1992. Temperature dependence and Arrhenius activation energy of F-actin velocity generated in vitro by skeletal myosin. Journal of molecular biology 224:1029-1038.
31. Canepari, M., M. Maffei, E. Longa, M. Geeves, and R. Bottinelli. 2012. Actomyosin kinetics of pure fast and slow rat myosin isoforms studied by in vitro motility assay approach. Experimental physiology 97:873-881.

32. Pellegrino, M. A., M. Canepari, R. Rossi, G. D'Antona, C. Reggiani, and R. Bottinelli. 2003. Orthologous myosin isoforms and scaling of shortening velocity with body size in mouse, rat, rabbit and human muscles. The Journal of physiology 546:677-689.
33. Mijailovich, S. M., O. Kayser-Herold, B. Stojanovic, D. Nedic, T. C. Irving, and M. A. Geeves. 2016. Three-dimensional stochastic model of actin-myosin binding in the sarcomere lattice. The Journal of general physiology 148:459-488.
34. Geeves, M., H. Griffiths, S. Mijailovich, and D. Smith. 2011. Cooperative [Ca(2)+]-dependent regulation of the rate of myosin binding to actin: solution data and the tropomyosin chain model. Biophysical journal 100:2679-2687.
35. Smith, D. A., M. A. Geeves, J. Sleep, and S. M. Mijailovich. 2008. Towards a unified theory of muscle contraction. I: foundations. Ann Biomed Eng 36:1624-1640.
36. Smith, D. A., and S. M. Mijailovich. 2008. Toward a unified theory of muscle contraction. II: predictions with the mean-field approximation. Ann Biomed Eng 36:1353-1371.
37. Mijailovich, S. M., O. Kayser-Herold, X. Li, H. Griffiths, and M. A. Geeves. 2012. Cooperative regulation of myosin-S1 binding to actin filaments by a continuous flexible Tm-Tn chain. Eur Biophys J 41:1015-1032.
38. Mijailovich, S. M., X. Li, R. H. Griffiths, and M. A. Geeves. 2012. The Hill model for binding myosin S1 to regulated actin is not equivalent to the McKillop-Geeves model. Journal of molecular biology 417:112-128.
39. Prodanovic, M., T. C. Irving, and S. M. Mijailovich. 2016. X-ray diffraction from nonuniformly stretched helical molecules. J Appl Crystallogr 49:784-797.
40. Mijailovich, S. M., O. Kayser-Herald, R. L. Moss, and M. A. Geeves. 2009. Thin Filament Regulation of Relaxation in 3D Multi-Sarcomere Geometry Biophys J 96:201a (Abstract).
41. Mijailovich, S. M., B. Stojanovic, D. Nedic, and M. A. Geeves. 2015. Activation and Relaxation Kinetics in Skeletal and Cardiac Muscles. Biophysical journal 108:337a-338a.
42. Walklate, J., and M. A. Geeves. 2015. Temperature manifold for a stopped-flow machine to allow measurements from -10 to +40 degrees C. Analytical biochemistry 476:11-16.
43. Piroddi, N., A. Belus, B. Scellini, C. Tesi, G. Giunti, E. Cerbai, A. Mugelli, and C. Poggesi. 2007. Tension generation and relaxation in single myofibrils from human atrial

and ventricular myocardium. Pflugers Archiv : European journal of physiology 454:63-73.

44. Palmiter, K. A., M. J. Tyska, D. E. Dupuis, N. R. Alpert, and D. M. Warshaw. 1999. Kinetic differences at the single molecule level account for the functional diversity of rabbit cardiac myosin isoforms. The Journal of physiology 519 Pt 3:669-678.

45. Narolska, N. A., S. Eiras, R. B. van Loon, N. M. Boontje, R. Zaremba, S. R. Spiegelen Berg, W. Stooker, M. A. Huybregts, F. C. Visser, J. van der Velden, and G. J. Stienen. 2005. Myosin heavy chain composition and the economy of contraction in healthy and diseased human myocardium. Journal of muscle research and cell motility 26:39-48.

46. White, H. D., B. Belknap, and M. R. Webb. 1997. Kinetics of nucleoside triphosphate cleavage and phosphate release steps by associated rabbit skeletal actomyosin, measured using a novel fluorescent probe for phosphate. Biochemistry 36:11828-11836.

47. Heeley, D. H., B. Belknap, and H. D. White. 2002. Mechanism of regulation of phosphate dissociation from actomyosin-ADP-Pi by thin filament proteins. Proceedings of the National Academy of Sciences of the United States of America 99:16731-16736.

48. Liu, Y., H. D. White, B. Belknap, D. A. Winkelmann, and E. Forgacs. 2015. Omecamtiv Mecarbil modulates the kinetic and motile properties of porcine beta-cardiac myosin. Biochemistry 54:1963-1975.

49. Schiaffino, S., and C. Reggiani. 2011. Fiber types in mammalian skeletal muscles. Physiological reviews 91:1447-1531.

50. Siemankowski, R. F., M. O. Wiseman, and H. D. White. 1985. ADP dissociation from actomyosin subfragment 1 is sufficiently slow to limit the unloaded shortening velocity in vertebrate muscle. Proceedings of the National Academy of Sciences of the United States of America 82:658-662.

TABLE 1 Rate and equilibrium constants used for modeling the ATPase cycle.

Equilibrium Rate Const.	Units	Fast Skeletal	HC WT β-S1	HC WT α-S1	HC R453C-S1
Km		101.0	39.55	67.8	28.0
Vmax		29.3	5.94	18.0	5.0
K_A	μM^{-1}	**0.008**	**0.0107**	**0.011**	**0.012**
K_{Pi}	mM	100.0	100.0	100.0	100.0
K_D	μM	100.0	36.00	197.0	33.3
K_{D^*}	–	50.0	0.167	50.0	0.050
K_T	μM^{-1}	0.005	0.003	0.004	0.003
K_{T^*}	–	1507	154.0	150.0	150.0
$K_{T^{**}}$	μM	1000	1000	1000	1000
K_H	–	**10.22**	**8.9136**	**4.061**	**7.419**
K_{AH}	–	**75.15**	**63.145**	**52.76**	**150.3**

Forward Rate Const.	Units	Fast Skeletal	HC WT β-S1	HC WT α-S1	HC R453C-S1
k_A	$\mu M^{-1}s^{-1}$	**3.819**	**10.75**	**10.68**	**11.87**
k_{Pi}	s^{-1}	**45.25**	**15.95**	**32.14**	**17.58**
k_D	s^{-1}	1000	1000	1970	1000
k_{D^*}	s^{-1}	300.0	59.0	100.0	39.70
k_T	$\mu M^{-1}s^{-1}$	**7.785**	**10.05**	**27.57**	**10.72**
k_{T^*}	s^{-1}	1507	1543	1800	1500
$k_{T^{**}}$	s^{-1}	1000	1000	1000	1000
k_H	s^{-1}	**143.1**	**12.47**	**77.17**	**10.39**
k_{AH}	s^{-1}	**150.3**	**12.63**	**79.14**	**10.52**

Backward Rate Const.	Units	Fast Skeletal	HC WT β-S1	HC WT α-S1	HC R453C-S1
k_{-A}	s^{-1}	500	1000	1000	1000
k_{-Pi}	$mM^{-1}\ s^{-1}$	**0.452**	**0.159**	**0.321**	**0.176**
k_{-D}	$\mu M^{-1}\ s^{-1}$	10.0	27.80	10.0	30.3
k_{-D^*}	s^{-1}	6.0	354.0	2.0	794.0
k_{-T}	s^{-1}	**1557**	**3349**	**6597**	**3350**
k_{-T^*}	s^{-1}	1.0	10.0	12.0	10.0
$k_{-T^{**}}$	$\mu M^{-1}\ s^{-1}$	1.0	1.0	1.0	1.0
k_{-H}	s^{-1}	14.0	1.4	19.0	1.4
k_{-AH}	s^{-1}	2.0	0.2	1.50	0.07

[ATP] = 5mM , [ADP] = [Pi] = 0 mM (standard initial rate ATPase conditions).

Numbers in bold (black) were obtained from fits to the ATPase data shown in Fig 2A & 3A. The rest of the values were assigned as described in the methods section. Bold gray numbers are calculated from fitted values in bold black.

TABLE 2 Resolution matrix for the β-cardiac isoform

HC WT β– S1			K_A	k_{-Pi}	k_{-T}	K_H	K_{AH}
K_A	**0.0107**	μM^{-1}	0.**9092**	0.3125	-0.0001	-0.2264	-0.2320
k_{-Pi}	**0.159**	$s^{-1}mM^{-1}$	0.3125	**0.9586**	0.0001	0.2510	0.2524
k_{-T}	**3349**	s^{-1}	-0.0001	0.0001	**1.4×10^{-6}**	0.0002	0.0002
K_H	**8.91**	–	-0.2264	0.2510	0.0002	**0.8109**	-0.1840
K_{AH}	**63.14**	–	-0.2320	0.2524	0.0002	-0.1840	**0.8117**

TABLE 3 The resolution matrix diagonal values, R_d, for each of the isoforms. Full tables are in the Supporting Material

	Units	Fast Skeletal	HC WT β-S1	HC WT α-S1	HC R453C-S1
$R_d(K_A)$	–	0.981	0.909	0.993	0.966
$R_d(k_{-Pi})$	–	0.953	0.959	0.997	0.910
$R_d(k_{-T})$	–	2.5×10^{-6}	1.4×10^{-6}	2.3×10^{-6}	0.15×10^{-6}
$R_d(K_H)$	–	0.849	0.811	0.960	0.856
$R_d(K_{AH})$	–	0.813	0.812	0.981	0.858
Error	s^{-1}	7.050×10^{-6}	1.430×10^{-6}	7.060×10^{-6}	2.310×10^{-6}

TABLE 4 Effect of actin concentration on the fractional occupancy of ATPase cycle intermediates

	ATPase (s^{-1})	Detach.	Weak Att	Strong Att	Duty ratio	Velocity ($\mu m\ s^{-1}$)
Fast Skeletal						
[A]= **Km = 101 μM**	14.7353	0.5775	0.3478	0.0747	0.0747	0.9862
[A]= 3Km	22.0896	0.3498	0.5382	0.1120	0.1120	0.9860
[A]= 20Km	28.0331	0.1049	0.7529	0.1422	0.1422	0.9857
HC WT β - S1						
[A]= **Km = 39.55 μM**	2.9744	0.7263	0.2002	0.0734	0.0734	0.2023
[A]=3Km	4.4614	0.5655	0.3241	0.1103	0.1103	0.2021
[A]=20Km	5.6619	0.2984	0.5606	0.1410	0.1410	0.2008
HC WT α - S1						
[A]= **Km = 67.8 μM**	9.0033	0.5985	0.3013	0.1001	0.1001	0.4497
[A]=3Km	13.5034	0.3820	0.4676	0.1504	0.1504	0.4489
[A]=20Km	17.1395	0.1355	0.6732	0.1914	0.1914	0.4477
HC R453C β - S1						
[A]= **Km = 28 μM**	2.5013	0.7298	0.1528	0.1174	0.1174	0.1065
[A]=3Km	3.7525	0.5769	0.2468	0.1763	0.1763	0.1064
[A]=20Km	4.7601	0.3365	0.4389	0.2246	0.2246	0.1060

Detached = MT & MDPi, weakly attached = A-MT + A-MDPi, strongly attached = duty ratio DR = AMD + AM-D + AM + AMT.

Velocity = $d \times ATPase/DR$ where d = 5 nm.

TABLE 5 Predicted effect of load on the ATPase cycle when the actin concentration is 3Km

	ATPase (s^{-1})	Detach.	Weak Att	Strong Att	Duty ratio	Velocity ($\mu m\ s^{-1}$)	Δ% AMD	Δ % Velocity	Δ % ATPase
Fast Skeletal									
[A]= 3Km	22.0896	0.3498	0.5382	0.1120	0.1120	0.9860			
[A]= 3Km - loaded	8.5232	0.3130	0.5866	0.1004	0.1004	0.4245	15.75	-56.9	-61.4
HC WT β - S1									
[A]=3Km	4.4614	0.5655	0.3241	0.1103	0.1103	0.2021			
[A]=3Km - loaded	1.9720	0.4677	0.3930	0.1393	0.1393	0.0708	32.52	-64.9	-55.7
HC WT α - S1									
[A]=3Km	13.5034	0.3820	0.4676	0.1504	0.1504	0.4489			
[A]=3Km - loaded	5.1737	0.3305	0.5082	0.1612	0.1612	0.1605	14.94	-64.2	-61.4
HC R453C β - S1									
[A]=3Km	3.7525	0.5769	0.2468	0.1763	0.1763	0.1064			
[A]=3Km - loaded	1.6619	0.4714	0.3003	0.2283	0.2283	0.0364	32.84	-65.7	-55.7

Detach/weak att/strong att – show fractional occupancy for detached, weakly attached and strongly attached sates.

Duty ratio – fraction of strongly attached myosins/total myosin heads.

Δ% – % change in the parameter described on applying a load.

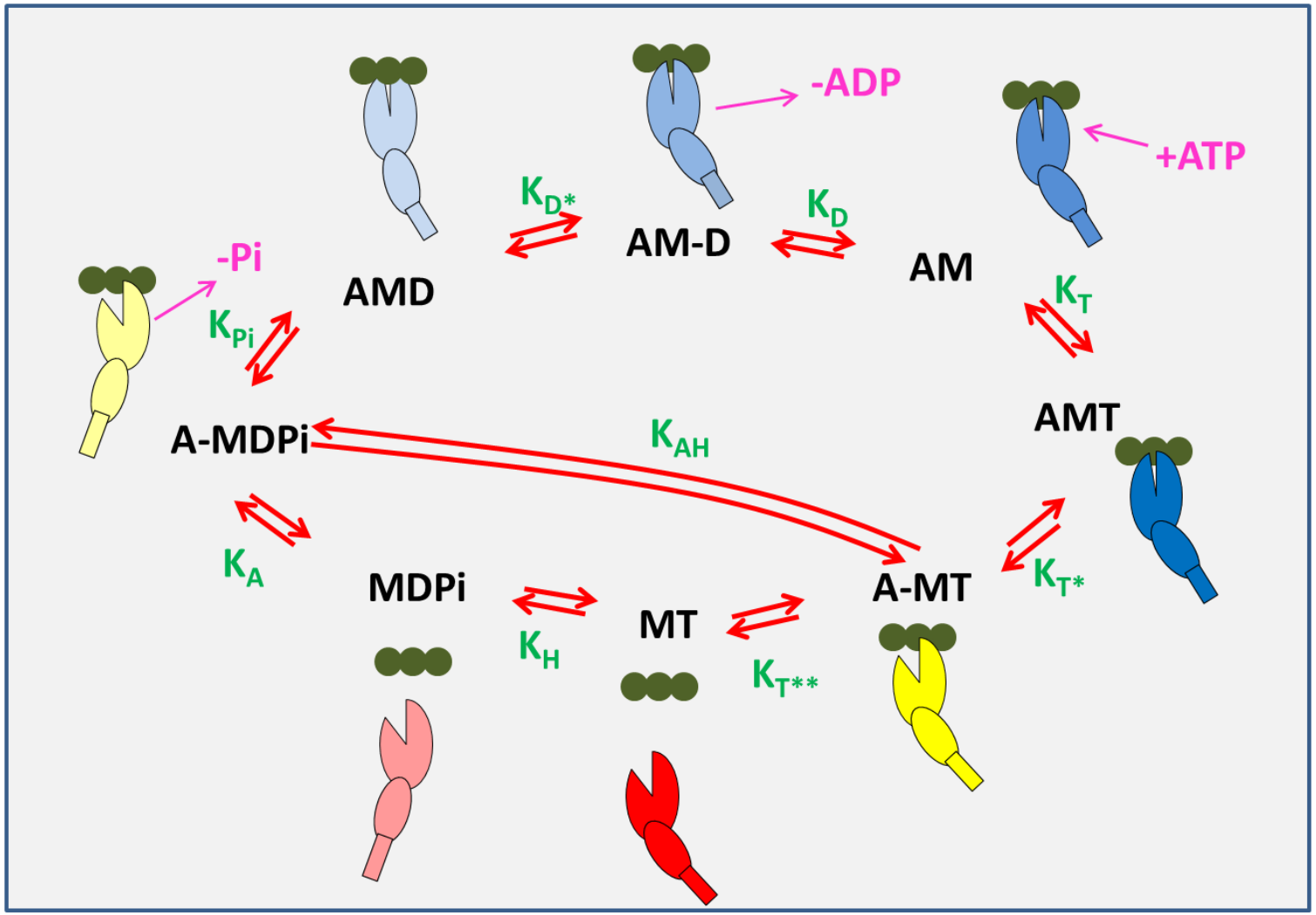
-ADP
+ATP
K_{D*}
K_D
AM-D
AM
AMD
-Pi
K_{Pi}
K_T
AMT
A-MDPi
K_{AH}
K_A
MDPi
K_H
MT
K_{T**}
A-MT
K_{T*}

FIGURE 1

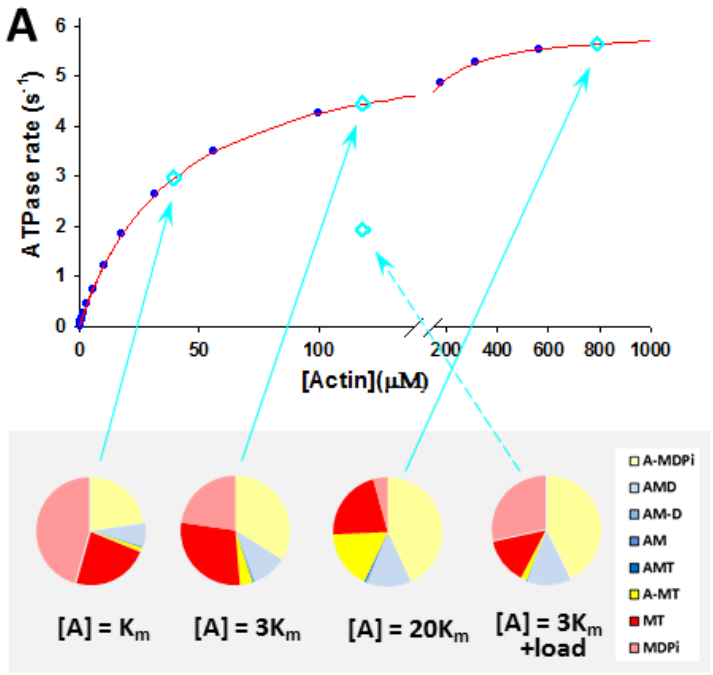
A
A TPase rate (s-1)
[Actin](μM)
A-MDPi
AMD
AM-D
AM
AMT
A-MT
MT
MDPi
[A] = Km
[A] = 3Km
[A] = 20Km
[A] = 3Km +load

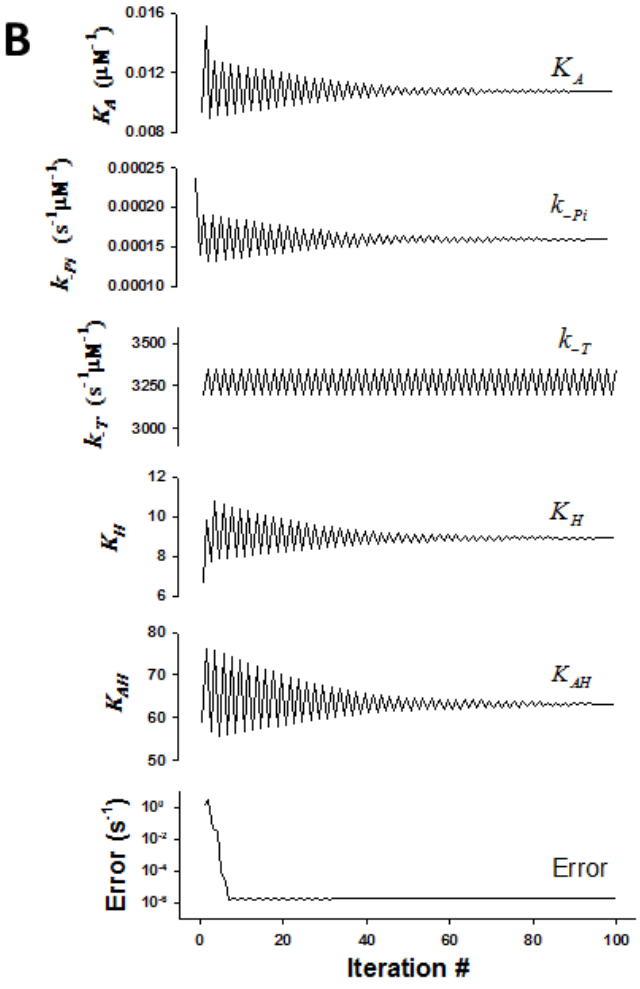
B
KA (μM-1)
k-Pi (s-1μM-1)
k-T (s-1μM-1)
KH
KAH
Error (s-1)
Iteration #

FIGURE 2

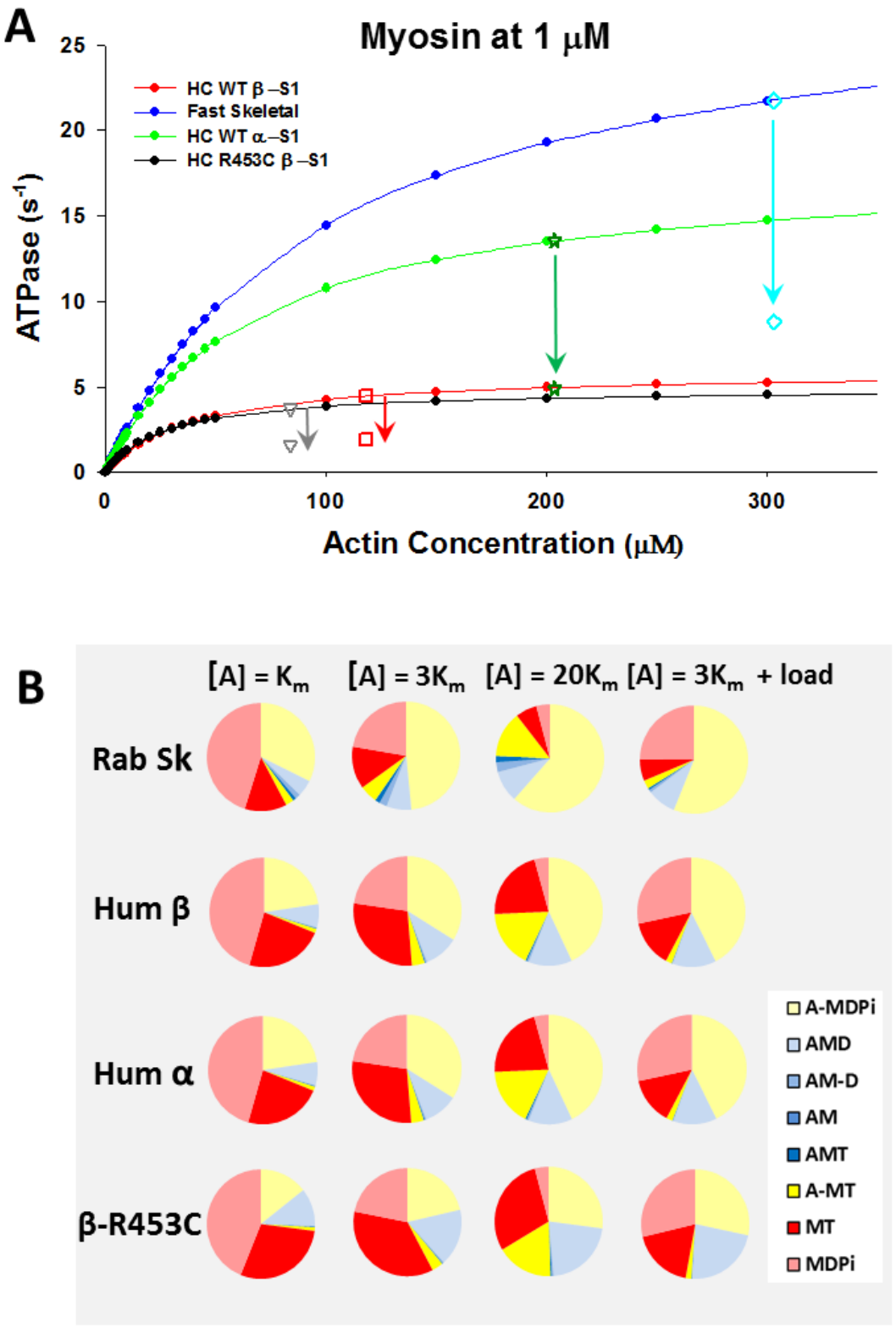
A
Myosin at 1 μM
HC WT β –S1
Fast Skeletal
HC WT α–S1
HC R453C β –S1
ATPase (s-1)
Actin Concentration (μM)
0
5
10
15
20
25
0
100
200
300
B
[A] = Km
[A] = 3Km
[A] = 20Km
[A] = 3Km + load
Rab Sk
Hum β
Hum α
β-R453C
A-MDPi
AMD
AM-D
AM
AMT
A-MT
MT
MDPi

FIGURE 3

SUPPORTING MATERIAL

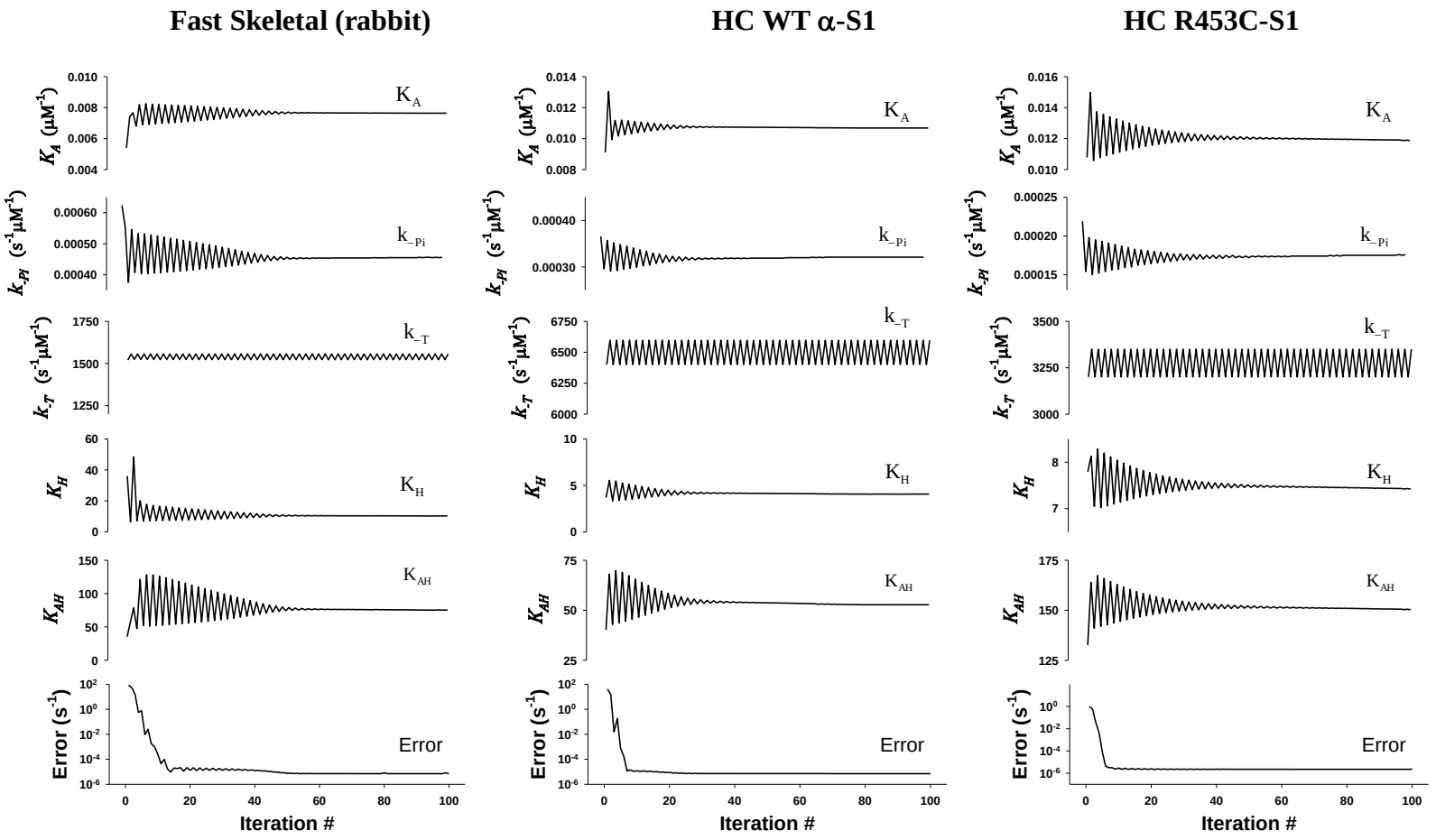

FIGURE S1 Convergence of fitted parameters for rabbit fast skeletal, human cardiac α-S1 and human cardiac β-R453C-S1

TABLE S1 Rate and equilibrium constants for the 3 myosin isoforms and one β-cardiac myosin mutant. At 100 and 25 mM KCl

	Units	Fast Skeletal		HC WT β		HC WT* α	HC WT α	β-R453C*	β-R453C
		25 mMKCl	100 mM KCl	25 mM KCl	100 mM KCl	25 mM KCl	100 mM KCl	25 mM KCl	100 mM KCl
K_A	mM^{-1}	**7.08**	**2.0**	**10.7**	**4.0**	**?**	**11.30**	**?**	**14.35**
K_{Pi}	mM	**100**	**?**	**100**	**?**	**?**	**100**	**?**	**100**
K_D	μM	100	120	36	170	197	152	33	100.00
K_{D^*}	–	50	50	0.1667	0.14	50	83.33	0.05	0.046
K_T	mM^{-1}	5	1.92	3	0.88	4.1	1.6	3.2	1.1
K_{T^*}	–	1507	1250	154.30	144	150.00	150.00	150	124.80
$K_{T^{**}}$	μM	1000	1000	1000	1000	1000	1000	1000	1000
K_H	–	**5**	**5.5**	**8.91**	**5.6**	**5**	**8.52**	**1.8**	2.86
K_{AH}	–	**61.77**	**?**	**63.14**		**63.3**	**99.60**	**?**	124.43
K_m	μM	**101.0**[1]	-	**39.55**[3]	-	**67.8**		**28**[4]	
V_{max}	s^{-1}	**29.3**[1]	-	**5.94**[3]	-	**18**		**5**[4]	
Forward Rate Constants									
k_A	$\mu M^{-1}s^{-1}$	**3.54**	**1**	**10.75**	**4**	**?**	**11.30**	**?**	**14.35**
k_{Pi}	s^{-1}	**49.67**	**?**	**15.95**	**?**	**?**	**27.20**	**?**	**14.69**
k_D	s^{-1}	1000	1200	1000	1000	1970	1520	1000	1000
k_{D^*}	s^{-1}	300	300	59.00	93	100	100.00	39.69	63.00
k_T	$\mu M^{-1}\ s^{-1}$	**7.7**	**10**	**10.00**	**3.33**	**27.2**	**10.51**	**10**	**3.3**
k_{T^*}	s^{-1}	1507	1250	1543	1445	1800	1500	1500	1248
$k_{T^{**}}$	s^{-1}	1000	1000	1000	1000	1000	1000	1000	1000
k_H	s^{-1}	**70**	**110**	**12.47**	**14**	**95.1**	**143.16**	**2.52**	**4**
k_{AH}	s^{-1}	**123.54**	**?**	**12.63**	**?**		**149.40**		**8.71**
Backward Rate Constants									
k_{-A}	s^{-1}	500	500	1000	1000		1000	?	1000
k_{-Pi}	$mM^{-1}\ s^{-1}$	**0.5**	**0.5**	**0.15**			**0.27**	**?**	**0.15**
k_{-D}	$\mu M^{-1}\ s^{-1}$	10	10	27.8	5.9	10	10	30.3	10
k_{-D^*}	s^{-1}	6	6	354	650		1.20	794	1369
k_{-T}	s^{-1}	**1540**	**5208**	**3349**	**3784**	**6500**	**6541.53**	**3125**	**3000**
k_{-T^*}	s^{-1}	1	1	10	10	12	10	10	10.00
$k_{-T^{**}}$	$\mu M^{-1}\ s^{-1}$	1	1	1	1	1	1	1	1
k_{-H}	s^{-1}	14	20	1.4	2.5	19	16.8	1.4	1
k_{-AH}	s^{-1}	2	?	0.2	?	?	1.5	?	0.07

For the ATPase assays
[ATP] = 5mM , [ADP] = [Pi] = 0 mM (standard initial rate ATPase conditions).
[S1] = 1 µM with varied [actin].
Conditions: 25 mM KCl, 20 mM MOPS, 5 mM $MgCl_2$ unless otherwise stated.

Source of Data
Bold allowed to vary in the fit to ATPase data
X Assumed diffusion limited:
X Assumed min/max value
X From detailed balance $K_i = k_i/k_{-i}$
X From transients
X from ATPase data reference:

NB the data for HC α WT and R453C at 25 mM KCl is estimated from the 100 mM data and the KCl dependence of the valued for the rabbit fast and HC-β muscle isoforms.

1: Swenson, A.M., Trivedi, D.V., Rauscher, A.A., Wang, Y., Takagi, Y., Palmer, B.M., Málnási-Csizmadia, A., Debold, E.P., Yengo, C. M. Magnesium modulates actin binding and ADP release in myosin motors. The Journal of Biological Chemistry, 2014, 289 (34) pp 23977-91.

IIa from rabbit

2: Nyitrai, M., Rossi, R., Adamek, N., Pellegrino, M.A., Bottinelli, R., Geeves, M. A. What limits the velocity of fast-skeletal muscle contraction in mammals? Journal of Molecular Biology, 2006, 355 (3) 432-42

This work gives values of k_2 (= 740 s^{-1}) and $1/K_T$ (= 520 µM) at 12 C. The value of $1/K_T$ is independent of temperature so the value of k_2 at 20 C can be estimated from the $K_T k_2$ value at 20 C. Thus $K_T k_2$= 2.4 $uM^{-1}s^{-1}$ where K_T = 0.00192 µM and k_2 = 1,248 s^{-1}.

3: Nag, S., Sommese, R.F., Ujfalusi, Z., Combs, A., Langer, S., Sutton, S., Leinwand, L. A., Geeves, M. A., Ruppel, K. M., Spudich, J. A. Contractility parameters of human β-cardiac myosin with the hypertrophic cardiomyopathy mutation R403Q show loss of motor function. Sci Adv. 2015 Oct 9;1(9):e1500511. doi: 10.1126/sciadv.1500511
4: Sommese R.F., Sung J., Nag S., Sutton S. Deacon J.C.Choe E., Leinwand L.A., Ruppel K., Spudich J.A. Molecular consequences of the R453C hypertrophic cardiomyopathy mutation on human β-cardiac myosin motor function. Proc Natl Acad Sci U S A. 2013 Jul 30;110(31):12607-12. doi: 10.1073/pnas.1309493110

Table S2 State occupancies of intermediates in the crossbridge cycle for the four myosins used here as a function of actin concentration and load.

	A-MDPi	AMD	AM-D	AM	AMT	A-MT	MT	MDPi	ATPase (s^{-1})	Detach.	Weak Att	Strong Att	Duty ratio	Δ% AMD with load	Velocity (μm/s)
Fast Skeletal															
[A]= Km = 101 μM	0.3234	0.0494	0.0147	0.0008	0.0098	0.0244	0.1260	0.4515	14.7353	0.5775	0.3478	0.0747	0.0747		0.9862
[A]= 3Km	0.4848	0.0741	0.0221	0.0012	0.0147	0.0534	0.1269	0.2229	22.0896	0.3498	0.5382	0.1120	0.1120		0.9860
[A]= 20Km	0.6152	0.0940	0.0280	0.0015	0.0187	0.1377	0.0639	0.0410	28.0331	0.1049	0.7529	0.1422	0.1422		0.9857
[A]= 3Km - loaded	0.5611	0.0857	0.0085	0.0004	0.0057	0.0255	0.0649	0.2481	8.5232	0.3130	0.5866	0.1004	0.1004	15.75	0.4245
HC WT β - S1															
[A]= Km = 39.55 μM	0.1865	0.0683	0.0030	0.0002	0.0020	0.0138	0.2779	0.4484	2.9744	0.7263	0.2002	0.0734	0.0734		0.2023
[A]=3Km	0.2797	0.1024	0.0045	0.0003	0.0032	0.0444	0.3423	0.2232	4.4614	0.5655	0.3241	0.1103	0.1103		0.2021
[A]=20Km	0.3550	0.1299	0.0057	0.0004	0.0050	0.2056	0.2562	0.0422	5.6619	0.2984	0.5606	0.1410	0.1410		0.2008
[A]=3Km - loaded	0.3707	0.1357	0.0020	0.0001	0.0014	0.0224	0.1744	0.2933	1.9720	0.4677	0.3930	0.1393	0.1393	32.52	0.0708
HC WT α - S1															
[A]= Km = 67.8 μM	0.2801	0.0901	0.0046	0.0003	0.0051	0.0212	0.1988	0.3997	9.0033	0.5985	0.3013	0.1001	0.1001		0.4497
[A]=3Km	0.4201	0.1352	0.0069	0.0005	0.0078	0.0475	0.1833	0.1987	13.5034	0.3820	0.4676	0.1504	0.1504		0.4489
[A]=20Km	0.5333	0.1716	0.0087	0.0006	0.0105	0.1399	0.0982	0.0373	17.1395	0.1355	0.6732	0.1914	0.1914		0.4477
[A]=3Km - loaded	0.4829	0.1554	0.0026	0.0002	0.0030	0.0253	0.1058	0.2247	5.1737	0.3305	0.5082	0.1612	0.1612	14.94	0.1605
HC R453C β - S1															
[A]= Km = 28 μM	0.1423	0.1130	0.0025	0.0002	0.0017	0.0105	0.2904	0.4394	2.5013	0.7298	0.1528	0.1174	0.1174		0.1065
[A]=3Km	0.2134	0.1696	0.0038	0.0002	0.0027	0.0334	0.3584	0.2185	3.7525	0.5769	0.2468	0.1763	0.1763		0.1064
[A]=20Km	0.2707	0.2151	0.0048	0.0004	0.0043	0.1682	0.2953	0.0412	4.7601	0.3365	0.4389	0.2246	0.2246		0.1060
[A]=3Km - loaded	0.2835	0.2253	0.0017	0.0001	0.0012	0.0168	0.1837	0.2877	1.6619	0.4714	0.3003	0.2283	0.2283	32.84	0.0364

TABLE S3: Resolution matrices for Fast Skeletal (Rabbit), HC WT α-S1 and HC R 452C β-S1

HF-Sk S1			K_A	k_{Pi}	k_{-T}	K_H	K_{AH}
K_A	**0.008**	–	**0.98105**	0.02946	-0.00102	-0.09029	-0.09531
k_{-Pi}	**0.452**	$mM^{-1}\ s^{-1}$	0.02946	**0.95335**	0.00107	0.14446	0.15064
k_{-T}	**1557**	$s^{-1}\mu M^{-1}$	-0.00102	0.00107	**2.5×10^{-6}**	0.00024	0.00030
K_H	**10.22**	μM^{-1}	-0.09029	0.14446	0.00024	**0.84917**	-0.46562
K_{AH}	**75.15**	μM^{-1}	-0.09531	0.15064	0.00030	-0.46562	**0.81309**

HC WT-α S1			K_A	k_{Pi}	k_{-T}	K_H	K_{AH}
K_A	**0.011**	–	**0.99340**	0.01164	-0.00051	-0.04754	-0.05355
k_{-Pi}	**0.321**	$mM^{-1}\ s^{-1}$	0.01164	**0.99653**	-0.00018	0.01166	0.00802
k_{-T}	**6597**	$s^{-1}\mu M^{-1}$	-0.00051	-0.00018	**2.3×10^{-6}**	0.00097	0.00103
K_H	**4.061**	μM^{-1}	-0.04754	0.01166	0.00097	**0.95986**	-0.02654
K_{AH}	**52.76**	μM^{-1}	-0.05355	0.00802	0.00103	-0.02654	**0.98087**

HC R452C-β S1			K_A	k_{Pi}	k_{-T}	K_H	K_{AH}
K_A	**0.012**	–	**0.96580**	0.35804	-0.00010	-0.21072	-0.21505
k_{-Pi}	**0.176**	$mM^{-1}\ s^{-1}$	0.35804	**0.90917**	0.00009	0.23395	0.23350
k_{-T}	**3349**	$s^{-1}\mu M^{-1}$	-0.00010	0.00009	**0.15×10^{-6}**	0.00014	0.00015
K_H	**7.419**	μM^{-1}	-0.21072	0.23395	0.00014	**0.85566**	-0.13811
K_{AH}	**150.3**	μM^{-1}	-0.21505	0.23350	0.00015	-0.13811	**0.85850**

TABLE S4: Sensitivity analysis of the fitted parameters to change of +20% or -20% fixed parameters k_{-D}, K_{D^*} , $k_{D^*}$and K_{-T^*} for HC WT β - S1.

	Units	Estimated constants	Fixed k_{-D}		Fixed K_{D^*}		Fixed k_{-D^*}		Fixed K_{-T^*}		Fixed $k_{-T^{**}}$	
			K_D +20%	K_D -20%	k_{D^*} +20%	k_{D^*} -20%	k_{D^*} +20%	k_{D^*} -20%	k_{-T^*} +20%	k_{-T^*} -20%	$K_{-T^{**}}$ +20%	$K_{-T^{**}}$-20%
K_A	μM^{-1}	**0.01075**	**0.47%**	**-2.33%**	**2.33%**	**-5.12%**	**3.26%**	**-6.98%**	**0.93%**	**-1.40%**	**3.26%**	**-0.47%**
K_{Pi}	mM	100	0.00%	0.00%	0.00%	0.00%	0.00%	0.00%	0.00%	0.00%	0.00%	0.00%
K_T	μM^{-1}	0.003	0.00%	0.00%	0.00%	0.00%	0.00%	0.00%	0.00%	0.00%	0.00%	0.00%
K_H	–	**8.9136**	**-1.48%**	**0.30%**	**-2.16%**	**1.04%**	**-2.55%**	**1.83%**	**-0.51%**	**0.20%**	**0.97%**	**-0.47%**
K_{AH}	–	**63.145**	**-1.48%**	**0.33%**	**-2.18%**	**1.06%**	**-2.57%**	**1.86%**	**-0.63%**	**0.20%**	**0.98%**	**-0.41%**
Forward Rate Constants												
k_A	$\mu M^{-1}s^{-1}$	**10.75**	**0.47%**	**-2.33%**	**2.33%**	**-5.12%**	**3.26%**	**-6.98%**	**0.93%**	**-1.40%**	**3.26%**	**-0.47%**
k_{Pi}	s^{-1}	**15.95**	**-0.31%**	**2.19%**	**-2.19%**	**5.33%**	**-2.82%**	**6.58%**	**-0.31%**	**0.94%**	**-3.45%**	**0.31%**
k_T	$\mu M^{-1}s^{-1}$	**10.048**	**0.00%**	**0.00%**	**0.00%**	**0.00%**	**0.00%**	**0.00%**	**0.00%**	**0.00%**	**0.01%**	**0.00%**
k_H	s^{-1}	**12.479**	**-1.48%**	**0.32%**	**-2.16%**	**1.04%**	**-2.55%**	**1.83%**	**-0.51%**	**0.20%**	**0.97%**	**-0.47%**
k_{AH}	s^{-1}	**12.629**	**-1.49%**	**0.33%**	**-2.18%**	**1.06%**	**-2.57%**	**1.86%**	**-0.63%**	**0.20%**	**0.98%**	**-0.41%**
Backward Rate Constants												
k_{-A}	s^{-1}	1000	0.00%	0.00%	0.00%	0.00%	0.00%	0.00%	0.00%	0.00%	0.00%	0.00%
k_{-Pi}	$mM^{-1}s^{-1}$	**0. 159**	**-0.31%**	**2.19%**	**-2.19%**	**5.33%**	**-2.82%**	**6.58%**	**-0.31%**	**0.94%**	**-3.45%**	**0.31%**
k_{-T}	s^{-1}	**3349.37**	**0.00%**	**0.00%**	**0.00%**	**0.00%**	**0.00%**	**0.00%**	**0.00%**	**0.00%**	**0.01%**	**0.00%**
k_{-H}	s^{-1}	1.4	0.00%	0.00%	0.00%	0.00%	0.00%	0.00%	0.00%	0.00%	0.00%	0.00%
k_{-AH}	s^{-1}	0.2	0.00%	0.00%	0.00%	0.00%	0.00%	0.00%	0.00%	0.00%	0.00%	0.00%

Numbers in bold (black) were obtained from fits to the ATPase data shown in Fig 2A & 3A. The rest of the values were assigned as described in the methods section. Bold gray numbers are calculated from fitted values in bold black.

TABLE S5: The effect of change of k_H by ±20% on estimated parameters including k_{Pi}

	Units	Estimated constants	Fixed k_{-H}		Fixed k_{-H}	
			k_H +20%	k_H -20%	k_H +20%	k_H -20%
K_A	μM^{-1}	**0.01075**	**0.00758**	**0.0128**	**-29.51%**	**19.23%**
K_{Pi}	mM	100	100	100	0.00%	0.00%
K_T	μM^{-1}	0.003	0.003	0.003	0.00%	0.00%
K_H	–	8.9136	7.1257	10.696	20.00%	-20.00%
K_{AH}	–	**63.145**	**50.4133**	**75.888**	**-20.16%**	**20.18%**
Forward Rate Constants						
k_A	$\mu M^{-1}s^{-1}$	**10.75**	**7.578**	**12.82**	**-29.51%**	**19.23%**
k_{Pi}	s^{-1}	**15.950**	**23.290**	**13.129**	**46.02%**	**-17.77%**
k_T	$\mu M^{-1}s^{-1}$	**10.048**	**10.042**	**10.047**	**0.00%**	**0.00%**
k_H	s^{-1}	12.479	9.976	14.975	-20.00%	20.00%
k_{AH}	s^{-1}	**12.629**	**10.083**	**15.178**	**-20.16%**	**20.18%**
Backward Rate Constants						
k_{-A}	s^{-1}	1000	1000	1000	0.00%	0.00%
k_{-Pi}	$mM^{-1}s^{-1}$	**0. 159**	**0.233**	**0.131**	**46.48%**	**-17.51%**
k_{-T}	s^{-1}	**3349.37**	**3349.45**	**3349.17**	**0.00%**	**0.00%**
k_{-H}	s^{-1}	1.4	1.4	1.4	0.00%	0.00%
k_{-AH}	s^{-1}	0.2	0.2	0.2	0.00%	0.00%
Error	s^{-1}	1.43×10^{-6}	7.60×10^{-7}	1.76×10^{-6}		

Numbers in bold (black) were obtained from fits to the ATPase data shown in Fig 2A & 3A. The rest of the values were assigned as described in the methods section. Bold gray numbers are calculated from fitted values in bold black.

Table S6 Change of state occupancies of intermediates in the crossbridge cycle for HC WT β - S1 as a function of +/- 20% k_H at actin concentration Km= 39.55 μM.

	A-MDPi	AMD	AM-D	AM	AMT	A-MT	MT	MDPi	ATPase (s^{-1})	Detach	Weak Att	Strong Att	Duty ratio	Velocity (μm/s)
[A]= K_m	0.1865	0.0682	0.0029	0.0002	0.0020	0.0137	0.2777	0.4484	2.9750	0.7262	0.2002	0.0734	0.0734	0.2026
[A]=3K_m +20% k_H	0.2265	0.0681	0.0029	0.0002	0.0020	0.0119	0.2320	0.4561	2.9717	0.6881	0.2385	0.0733	0.0733	0.2026
[A]=20K_m –20% k_H	0.1275	0.0681	0.0029	0.0002	0.0020	0.0164	0.3452	0.4374	2.9714	0.7826	0.1439	0.0733	0.0733	0.2025